Masthead Logo

Smith ScholarWorks

Astronomy: Faculty Publications

Astronomy

11-12-2015

Narrow Na and K Absorption Lines Toward T Tauri Stars: Tracing the Atomic Envelope of Molecular Clouds

I. Pascucci
The University of Arizona

Suzan Edwards
Smith College, sedwards@smith.edu

M Heyer
University of Massachusetts Amherst

E. Rigliaco
Institute for Astronomy Zurich

L. Hillenbrand
California Institute of Technology

See next page for additional authors

Follow this and additional works at: https://scholarworks.smith.edu/ast_facpubs

Part of the Astrophysics and Astronomy Commons

Recommended Citation

Pascucci, I.; Edwards, Suzan; Heyer, M; Rigliaco, E.; Hillenbrand, L.; Gorti, U.; Hollenbach, D.; and Simon, M. N., "Narrow Na and K Absorption Lines Toward T Tauri Stars: Tracing the Atomic Envelope of Molecular Clouds" (2015). Astronomy: Faculty Publications, Smith College, Northampton, MA.
https://scholarworks.smith.edu/ast_facpubs/1

This Article has been accepted for inclusion in Astronomy: Faculty Publications by an authorized administrator of Smith ScholarWorks. For more information, please contact scholarworks@smith.edu

Authors

I. Pascucci, Suzan Edwards, M Heyer, E. Rigliaco, L. Hillenbrand, U. Gorti, D. Hollenbach, and M. N. Simon

This article is available at Smith ScholarWorks: https://scholarworks.smith.edu/ast_facpubs/1

The Astrophysical Journal, 814:14 (17pp), 2015 November 20 doi:10.1088/0004-637X/814/1/14

© 2015. The American Astronomical Society. All rights reserved.

NARROW Na AND K ABSORPTION LINES TOWARD T TAURI STARS: TRACING THE ATOMIC ENVELOPE OF MOLECULAR CLOUDS

I. Pascucci[1], S. Edwards[2], M. Heyer[3], E. Rigliaco[4], L. Hillenbrand[5], U. Gorti[6,7], D. Hollenbach[6], and M. N. Simon[1]
[1] Lunar and Planetary Laboratory, The University of Arizona, Tucson, AZ 85721, USA; pascucci@lpl.arizona.edu
[2] Five College Astronomy Department, Smith College, Northampton, MA 01063, USA
[3] Department of Astronomy, University of Massachusetts, Amherst, MA 01003-9305, USA
[4] Institute for Astronomy, ETH Zurich, Wolfgang-Pauli-Strasse 27, CH-8093 Zurich, Switzerland
[5] Department of Astronomy, California Institute of Technology, Pasadena, CA 91125, USA
[6] SETI Institute, Mountain View, CA 94043, USA
[7] NASA Ames Research Center, Moffett Field, CA 94035, USA

Received 2015 July 18; accepted 2015 October 5; published 2015 November 12

ABSTRACT

We present a detailed analysis of narrow Na I and K I absorption resonance lines toward nearly 40 T Tauri stars in Taurus with the goal of clarifying their origin. The Na I λ5889.95 line is detected toward all but one source, while the weaker K I λ7698.96 line is detected in about two-thirds of the sample. The similarity in their peak centroids and the significant positive correlation between their equivalent widths demonstrate that these transitions trace the same atomic gas. The absorption lines are present toward both disk and diskless young stellar objects, which excludes cold gas within the circumstellar disk as the absorbing material. A comparison of Na I and CO detections and peak centroids demonstrates that the atomic gas and molecular gas are not co-located, the atomic gas being more extended than the molecular gas. The width of the atomic lines corroborates this finding and points to atomic gas about an order of magnitude warmer than the molecular gas. The distribution of Na I radial velocities shows a clear spatial gradient along the length of the Taurus molecular cloud filaments. This suggests that absorption is associated with the Taurus molecular cloud. Assuming that the gradient is due to cloud rotation, the rotation of the atomic gas is consistent with differential galactic rotation, whereas the rotation of the molecular gas, although with the same rotation axis, is retrograde. Our analysis shows that narrow Na I and K I absorption resonance lines are useful tracers of the atomic envelope of molecular clouds. In line with recent findings from giant molecular clouds, our results demonstrate that the velocity fields of the atomic and molecular gas are misaligned. The angular momentum of a molecular cloud is not simply inherited from the rotating Galactic disk from which it formed but may be redistributed by cloud–cloud interactions.

Key words: circumstellar matter – ISM: clouds – ISM: individual objects (Taurus) – ISM: kinematics and dynamics – stars: formation – stars: kinematics and dynamics

1. INTRODUCTION

T Tauri stars (hereafter, TTSs) are pre-main-sequence optically visible stars named after the brightest member of this class of objects in the Taurus-Auriga molecular cloud (Joy 1942). Optical spectroscopy, and in particular the equivalent width of the Hα line, is traditionally used to distinguish between two main subgroups: *classical* and *weak-line* TTSs (CTTSs and WTTSs). CTTSs are accreting disk gas as evinced by broad (FWHM $\sim$ 100 km s^{-1}) permitted H and He lines tracing free-falling gas onto the star, and by optical/UV emission in excess of the stellar photosphere probing the accretion shock at the stellar surface (e.g., Alcalá et al. 2014). On the contrary, WTTSs have weaker emission lines with no evidence of ongoing accretion. Most WTTSs also lack IR excess emission and hence are defined as Class III objects, i.e., TTSs with no circumstellar disks (but some WTTSs have excess emission at longer wavelengths indicative of outer disks or dust belts; see, e.g., Cieza et al. 2013). CTTSs have excess emission at multiple infrared wavelengths, typically starting at near-IR (NIR) wavelengths, and are classified as Class II objects (e.g., Espaillat et al. 2014, pp. 497–520).

High-resolution ($R \sim$ 30,000) spectroscopy has been vital to identifying and understanding the complex processes associated with star and planet formation. In addition to accreting disk gas, CTTSs eject a fraction of this material, which removes excess angular momentum. Forbidden emission lines blueshifted from the stellar velocity by $\sim$100 km s^{-1} trace this phenomenon (see, e.g., Ray et al. 2007 for a review). Forbidden lines also show a second low-velocity component typically blueshifted by less than 10 km s^{-1} that has been associated with a slow wind whose origin is still debated (for a review see, e.g., Alexander et al. 2014, pp. 475–496; Natta et al. 2014). Finally, permitted lines, including the Hα line, often show complex morphologies indicating that they trace not only accretion but also outflowing material, such as winds originating within a few stellar radii (e.g., Mundt 1984). In this contribution we focus on the Na I and K I resonance lines of TTSs.

While K I lines are generally not discussed in the context of TTSs, several works have presented Na I resonance line profiles of CTTSs, focusing on the high accretors ($\dot{M} > 10^{-8}\,M_{\odot}$ yr^{-1}) such as DL Tau and DR Tau. The profiles are complex: in addition to emission, most spectra present absorption features that vary in width from being unresolved ($\leqslant$10 km s^{-1}) to $\sim$100 km s^{-1} (e.g., Mundt 1984; Edwards et al. 1994). Natta & Giovanardi (1990) proposed that outflowing winds from the star can explain the P Cygni profile detected in about 20% of the Na I lines of CTTSs, usually the most active ones. However, broad ($\sim$100 km s^{-1}) Na I emission profiles as observed in BP Tau are most likely probing free-falling accreting gas similar to the Balmer lines (e.g., Muzerolle et al. 1998). The most common feature in the Na I lines of TTSs is a narrow ($\leqslant$10 km s^{-1}) sharp absorption close to the stellar radial velocity (RV) tracing material physically in front of the star. The absorber has been usually associated with cold interstellar medium (ISM) gas (e.g., Mundt 1984), although a circumstellar disk could not be ruled out with the available data (e.g., Appenzeller et al. 2005). A circumstellar origin would be especially interesting in the context of giant exoplanet atmospheres by providing a tracer of disk gas cooler than that being accreted onto the central star, gas that might be accreted onto the giant planets forming in the disk.

Recent transiting observations of hot Jupiters have found that the sodium-to-potassium abundance ratio in the atmosphere of these giant planets can be very different from the solar ratio (e.g., Sing et al. 2015). Detailed theoretical models of planetary atmospheres demonstrate that photochemistry cannot explain such different ratios, and drastic changes to atmospheric temperature profiles or clouds are not supported by the data (e.g., Lavvas et al. 2014). It is suggested that disk evolution might change the Na/K abundance ratios of the gas that giant planets accrete during formation. This hypothesis may be testable using optical spectroscopy of TTSs in different evolutionary stages once the origin of their sodium and potassium lines is established.

This paper focuses on understanding the origin of the narrow and sharp absorption in the Na I resonance profiles. Using high-resolution optical spectra for a sample of nearly 40 TTSs in Taurus spanning a range of evolutionary stages (Section 2), we show that (a) K I profiles present the same sharp absorptions seen in Na I profiles (Section 3) and (b) the absorption does not arise from gas in a circumstellar disk, nor from ISM gas, but rather from atomic gas surrounding the Taurus molecular cloud (Section 4). We also find that the atomic gas is more extended than the molecular gas, as traced by low-*J* CO rotational lines, and that its rotation axis is almost antiparallel to that of the Taurus molecular cloud. Our results, when combined with those on five giant molecular clouds in the Milky Way (Imara & Blitz 2011), argue against the hypothesis that molecular clouds simply inherit the velocity field and angular momentum of the rotating galactic disk out of which they formed.

2. OBSERVATIONS AND DATA REDUCTION

Observations were carried out with the Keck/HIRES spectrograph (Vogt et al. 1994) in two separate campaigns, in 2006 through the program C170Hr (PI, L. Hillenbrand) and in 2012 through the program N107Hr (PI: I. Pascucci). In both campaigns we used the red cross-disperser with the C5 decker and a $1\farcs1 \times 7''$ slit. This configuration covers the 4800–9000 Å spectral range at a resolution of 37,500 as measured from the width of four Th/Ar lines[8] near 5240 Å (but see below for our estimate of the spectral resolution). Exposure times for individual targets are summarized in Tables 1 and 2.

All science targets except TW Hya are known members of the Taurus-Auriga star-forming region (age ∼1 Myr, distance ∼140 pc; see, e.g., the review by Kenyon et al. 2008). TW Hya is a well-characterized star that is closer to us and belongs to a loose association (Torres et al. 2008). We keep it in our analysis as comparing its Na I and K I profiles to those of Taurus-Auriga members helps in understanding the origin of the narrow and sharp absorptions in these resonance lines. Targets from the 2006 campaign are mostly accreting classical TTSs with optically thick disks that extend inward close to the stellar surface (Class II spectral energy distribution [SED]); see Table 3. In 2012 we targeted more evolved systems, with lower accretion rates on average, as well as nonaccreting weak-line TTSs with transitional (small NIR but large mid-IR [MIR] and far-IR [FIR] excess emission) or no disks (Class III SED); see Table 4. Two sources, IP Tau and UX Tau A, were observed in both campaigns. The central stars span a large range in spectral type, from M4 to K0; see Tables 3 and 4 and Herczeg & Hillenbrand (2014) for a careful and homogeneous reclassification of Taurus sources and of TW Hya. Along with science targets, we acquired a set of O/B stars to remove telluric lines and photospheric standards (both belonging to the Taurus-Auriga star-forming region, as well as field dwarfs) to correct the science spectra from photospheric absorption features.

Table 1
2006 Campaign: Observation Log

Source	2MASSJ	Exposure Time
AA Tau	04345542+2428531	600
BP Tau	04191583+2906269	600
CW Tau	04141700+2810578	2700
CY Tau	04173372+2820468	900
DF Tau	04270280+2542223	300
DG Tau	04270469+2606163	300
DK Tau A	04304425+2601244	300
DL Tau	04333906+2520382	600
DO Tau	04382858+2610494	1200
DR Tau	04470620+1658428	900
GI Tau	04333405+2421170	900
GK Tau A	04333456+2421058	900
HN Tau A	04333935+1751523	900
IP Tau	04245708+2711565	300
TW Hya	11015191–3442170	600
UX Tau A	04300399+1813493	1200
V819 Tau	04192625+2826142	900

Table 2
2012 Campaign: Observation Log

Source	2MASSJ	Exposure Time
Anon 1	04132722+2816247	1480
CI Tau	04335200+2250301	2121
CoKu Tau4	04411681+2840000	7200
DH Tau A	04294155+2632582	3000
DM Tau	04334871+1810099	3600
DN Tau	04352737+2414589	899
DS Tau A	04474821+2925138	900
FM Tau	04141358+2812492	3600
FZ Tau	04323176+2420029	7200
GH Tau	04330622+2409339	1500
GM Aur	04551098+3021595	900
GO Tau	04430309+2520187	6202
HBC 427	04560201+3021037	600
HQ Tau	04354733+2250216	900
IP Tau	04245708+2711565	1500
IT Tau A	04335470+2613275	3710
UX Tau A	04300399+1813493	300
V1321 Tau	04325323+1735337	2603
V1348 Tau	04525707+1919504	600
V410 Tau	04183110+2827162	300
VY Tau	04391741+2247533	300
V710 Tau A	04315799+1821350	3600
V773 Tau	04141291+2812124	300
V836 Tau	05030659+2523197	2400

---

[8] http://www2.keck.hawaii.edu/inst/hires/slitres.html

Table 3
2006 Campaign: Source Properties Relevant to This Study

Source	SpTy	Multiplicity[a]	REF	TTSs	SED[b]	REF
AA Tau	M0.6	s	1, 2	C	II	2, 3
BP Tau	M0.5	s	1, 2	C	II	2, 3
CW Tau	K3	s	1, 2	C	II	2, 3
CY Tau	M2.3	s	1, 2	C	II	2, 3
DF Tau	M2.7	0.09	1, 2	C	II	2, 3
DG Tau	K7.0	s	1, 2	C	II	2, 3
DK Tau A	K8.5	2.30	1, 2	C	II	2, 3
DL Tau	K5.5	s	1, 2	C	II	2, 3
DO Tau	M0.3	s	1, 2	C	II	2, 3
DR Tau	K6	s	1, 2	C	II	2, 3
GI Tau	M0.4	s	1, 2	C	II	2, 3
GK Tau	K6.5	s	1, 2	C	II	2, 3
HN Tau A	K3	3.11	1, 2	C	II	2, 3
IP Tau	M0.6	s	1, 2	C	II	2, 3
UX Tau A	K0.0	2.63, 5.86	1, 2	C	T	2, 4
V819 Tau	K8.0	s	1, 2	W	II/III[c]	2, 3
TW Hya	M0.5	s	1, 5	C	T	6, 7

Notes.
[a] For multiple systems we give the separation in arcseconds from the primary.
[b] Known transition disks are marked with "T."
[c] This source has a weak infrared excess at wavelengths longer than 10 μm; it may be transitioning from Class II to III, but the excess is not as large as for classical transition disks (Furlan et al. 2009b).

References. (1) Herczeg & Hillenbrand 2014; (2) White & Ghez 2001; (3) Kenyon & Hartman 1995; (4) Furlan et al. 2009a; (5) Rucinski et al. 2008; (6) Dupree et al. 2012; (7) Calvet et al. 2002.

Table 4
2012 Campaign: Source Properties Relevant to This Study

Source	SpTy	Multiplicity[a]	REF	TTSs	SED[b]	REF
Anon 1	M0.5	s	1, 2	W	III	2, 3
CI Tau	K5.5	s[c]	1, 2	C	II	2, 3
CoKu Tau4	M1.1	0.05	1, 4	W	T	5, 6
DH Tau	M2.3	s	1, 2	C	II	2, 3
DM Tau	M3.0	s	1, 2	C	T	2, 6
DN Tau	M0.3	s	1, 2	C	II	2, 3
DS Tau	M0.4	s	1, 2	C	II	2, 3
FM Tau	M4.5	s	1, 2	C	II	2, 3
FZ Tau	M0.5	s	1, 2	C	II	2, 3
GH Tau	M2.3	0.31	1, 2	C	II	2, 3
GM Aur	K6.0	s	1, 2	C	T	2, 6
GO Tau	M2.3	s	1, 2	C	II	2, 3
HBC 427	K6.0	0.03	1, 7	W	II/III[d]	3, 8
HQ Tau	K2.0	s	1, 9	C	II	10, 11
IP Tau	M0.6	s	1, 2	C	II	2, 3
IT Tau A	K6.0	2.39	1, 2	C	II	2, 3
UX Tau A	K0.0	2.63, 5.86	1, 2	C	T	2, 6
VY Tau	M1.5	0.66	1, 2	W	II	2, 12
V410 Tau	K7	0.07	10, 2	W	III[e]	2, 12
V710 Tau A	M3.3	3.17	1, 2	C	II	2, 3
V773 Tau	K4.0	0.1[f]	1, 13	W	II	2, 11
V836 Tau	M0.8	s	1, 9	C	II	3, 14, 11
V1321 Tau	M2	s	10	W	III[g]	15, 16
V1348 Tau	K5	s	10	W	III	10, 17

Notes.
[a] For multiple systems we give the separation in arcseconds from the primary and the flux ratio to the primary when known.
[b] Known transition disks are marked with "T."
[c] Suspected SB1; Nguyen et al. (2012).
[d] This source has a weak infrared excess at wavelengths longer than 10 μm; it may be transitioning from Class II to III, but the excess is not as large as for classical transition disks (Furlan et al. 2006).
[e] Esplin et al. (2014) report a small excess in the *WISE* W2 band (4.6 μm) but note that the colors of V410 Tau are consistent with the stellar photosphere at longer wavelengths, as found in Furlan et al. (2006).
[f] The quoted separation is between the A and B components. A is a short-period (51 days) double-lined spectroscopic binary (Welty 1995). In addition, Duchene et al. (2003) and Woitas (2003) identified an additional infrared component (C) within $0\farcs3$ from A.
[g] Cieza et al. (2013) report excess at wavelengths longer than 24 μm for V1321 Tau (also known as RX J0432.8+1735). This source is thought to have a warm debris disk.

References. (1) Herczeg & Hillenbrand 2014; (2) White & Ghez 2001; (3) Kenyon & Hartmann 1995; (4) Ireland & Kraus 2008; (5) Cohen & Kuhi 1979; (6) Furlan et al. 2009a; (7) Steffen et al. 2001; (8) Kenyon et al. 1998; (9) Kraus et al. 2012; (10) Nguyen et al. 2009; (11) Furlan et al. 2011; (12) Furlan et al. 2006; (13) Ghez et al. 1993; (14) White & Hillebrand 2004; (15) Martin & Magazzu 1999; (16) Cieza et al. 2013; (17) Wichmann et al. 1996.

The data reduction was carried out using the highly automated Mauna Kea Echelle Extraction pipeline written by Tom Barlow.[9] The reduction steps included bias subtraction, flat-fielding, identification of the echelle orders on the images, and extraction of the spectra. Wavelength calibration was done using spectra of ThAr calibration lamps mounted on HIRES and acquired either right before or right after the target exposures. The reduction was performed in air wavelengths, using the keyword "novac" in the pipeline inputs. After spectral extraction, each of the individual one-dimensional spectra was rebinned to a linear wavelength scale. The final products of the reduction are wavelength-calibrated spectra to which heliocentric correction is also applied.

In this work we focus on the two orders that cover the Na D resonance line at 5889.95 Å and the K I line at 7698.96 Å.[10] Of these two orders, only that covering the K I line has strong telluric contamination; however, no telluric line overlaps with the lines of interest. After telluric removal, the set of nearby photospheric standards are used to subtract any photospheric absorption and identify those sources with Na and K emission. The removal of photospheric lines follows standard procedures (e.g., Hartigan et al. 1989). In brief, a photospheric standard with spectral type similar to that of the target star is chosen. When necessary, the standard photospheric lines are broadened to match those of the target, and the standard spectrum is shifted in wavelength to the target spectrum. The spectrum of the standard is also veiled to account for the extra emission known to fill in the absorption lines of young accreting stars. In practice, we veiled the standard spectrum by identifying a flat continuum and a normalization factor that best reproduce the target spectrum in a specified wavelength interval outside of the lines of interest. Finally, we divided the target spectrum by the broadened, veiled, and shifted spectrum of the standard. The photospheric standard GL846 (M0 SpTy) provided a good correction for all stars except three later-type M dwarfs (GH Tau, V710 Tau, V1321 Tau) and 11 K dwarfs (CI Tau, CW Tau, GK Tau, GM Aur, HBC 427, HN Tau, HQ Tau, IT Tau, UX Tau, V773 Tau, V1348 Tau). For the group of late M dwarfs the photospheric standard GL15 (M2 SpTy) was

---

[9] http://www2.keck.hawaii.edu/inst/common/makeewww/index.html

[10] The weaker Na D resonance line at 5895.92 Å is too close to the edge of the order, while the other K I resonance line at 7664.89 Å is not covered by our setting.

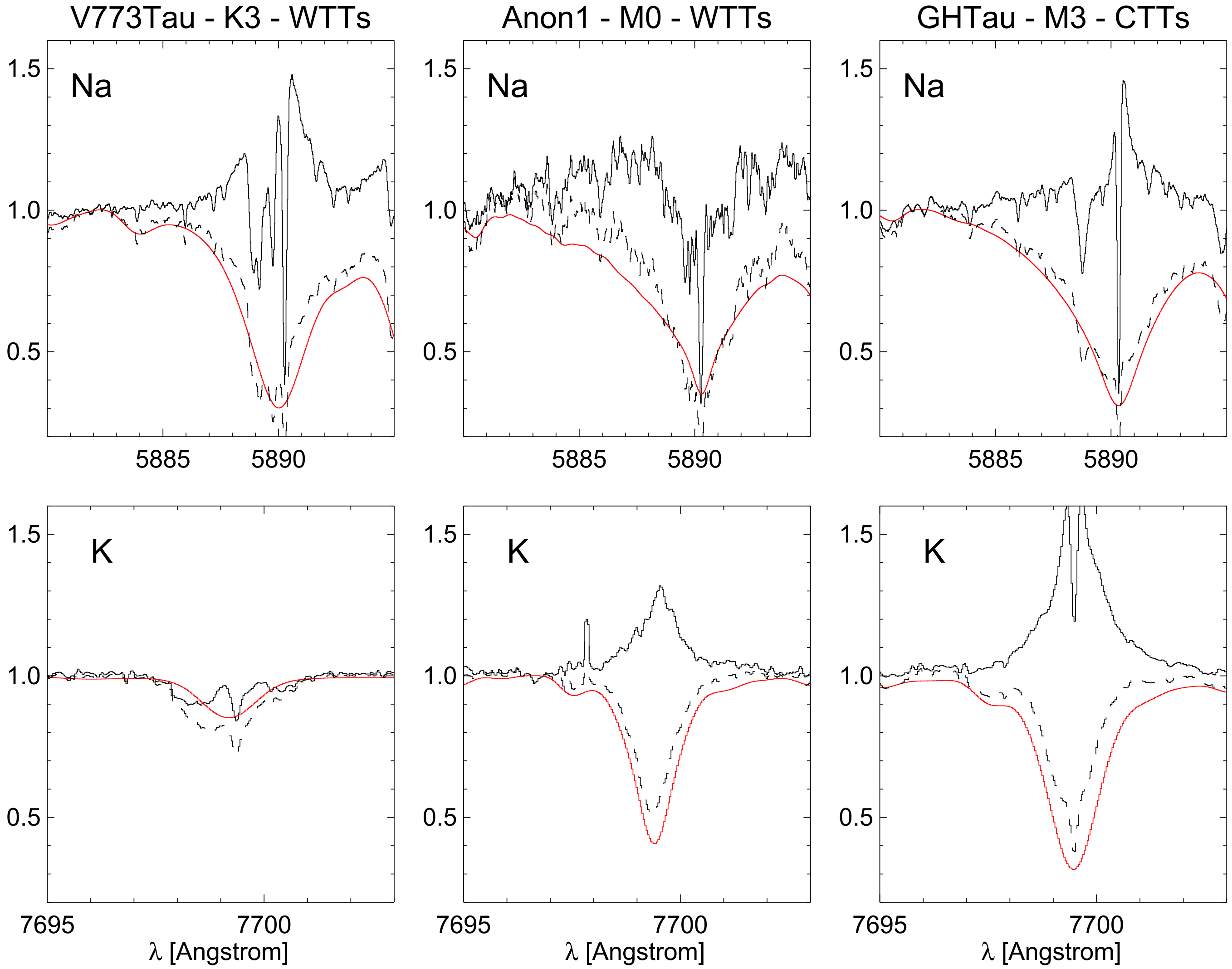

Figure 1. Sample of original Na and K spectra (dashed line), scaled/veiled and broadened photospheric standard spectra (red solid line), and residual profiles (black solid line). These stars are chosen to cover the large range of spectral type of our sample and both accreting (CTTSs) and nonaccreting (WTTSs) objects. Because Na and K lines are gravity sensitive, care should be taken in interpreting weak excess emission in the residual profiles, especially if the emission is as broad as that of photospheric lines. The figure also illustrates that the position and width of the narrow Na and K absorption features, which are the focus of this paper, are not affected by the photospheric subtraction.

used, while for the K dwarfs the standard HR 8832 (K3 SpTy) was applied. The approach described above produces residual line profiles. Care should be taken to interpret these profiles, especially weak and/or narrow excess emission, because Na I and K I photospheric lines are deep and gravity sensitive. However, nearby/older dwarfs are necessary to remove the photosphere because even WTTSs in Taurus present the deep Na I and K I absorption lines we want to investigate. To illustrate the difficulty in creating residual profiles, we show in Figure 1 the original spectra, the veiled/scaled and broadened photosphere, and the residual spectra for three stars with spectral type from early K (V773 Tau) to middle M (GH Tau) and covering both CTTSs and WTTSs. Residual profiles are typically less reliable for WTTSs than CTTSs. Further discussion of these profiles is provided in Section 3.1.

We also independently measured the spectral resolution achieved by HIRES in our observational setting using the strongest telluric lines in the order covering the K I resonance transition. The distribution of FWHMs for nearly 90 telluric lines from spectra obtained in the 2006 and 2012 campaigns is

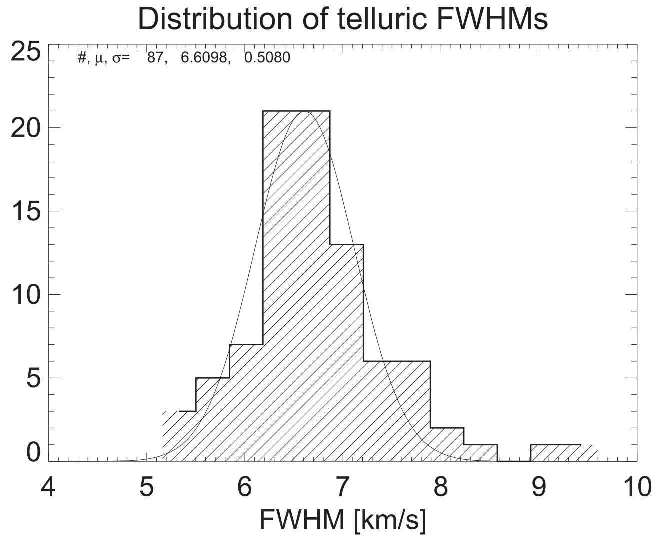

Figure 2. Distribution of FWHMs from nearly 90 telluric lines. A Gaussian fit to the distribution results in a mean FWHM of 6.6 km s^{-1}, corresponding to a spectral resolution of ∼45,000 and standard deviation of 0.5 km s^{-1}.

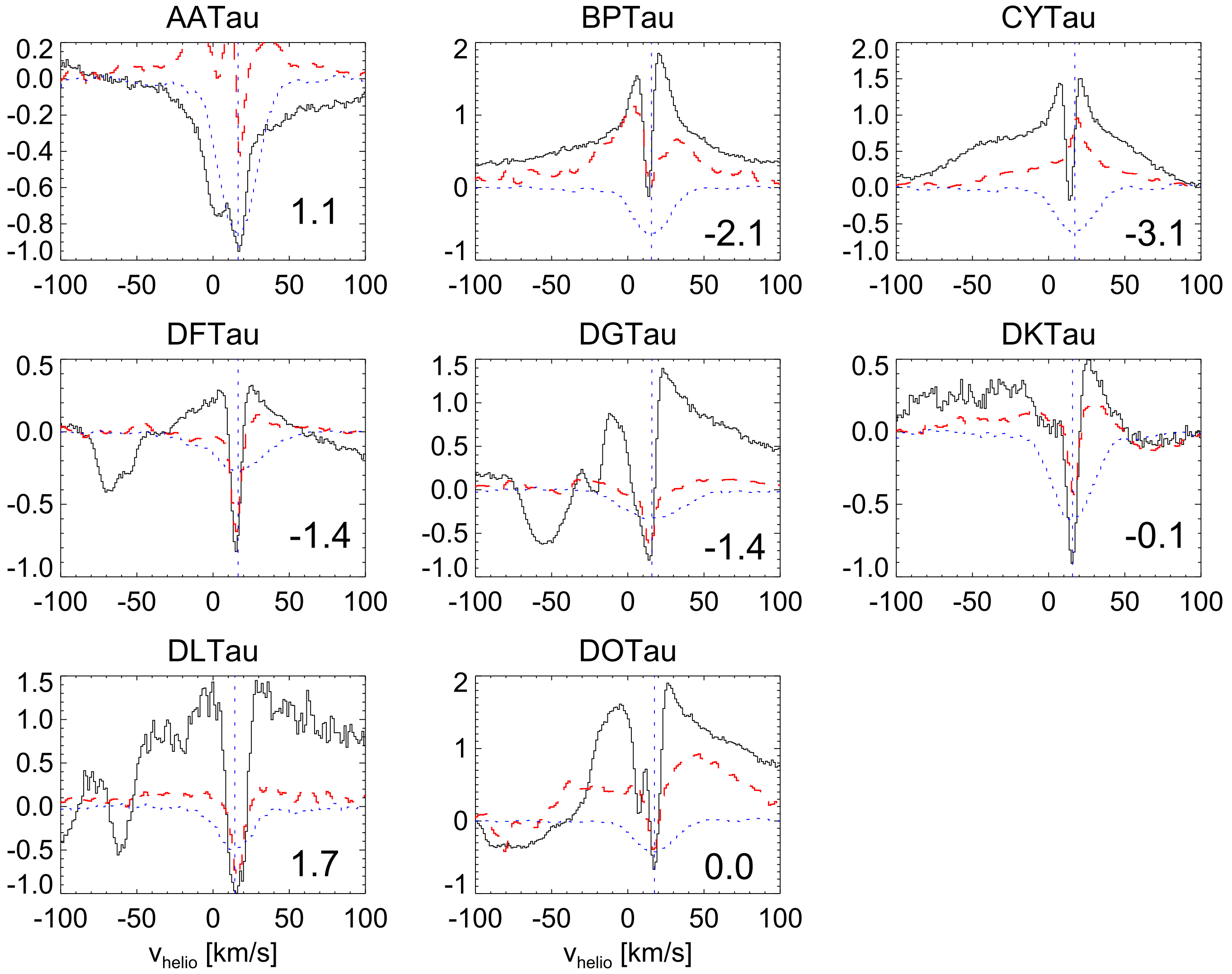

Figure 3. Residual Na I λ5890 (black solid line) and K I λ7699 (red dashed line) profiles for CTTSs. The *x*-axis gives heliocentric velocities. Dotted (blue) lines show the Li photospheric profile at 6707.83 Å and its centroid. The number in the lower right corner of each panel gives the difference between the narrow Na I absorption and the stellar RV measured from the Li line. The K I profiles of BP Tau and DO Tau are multiplied by a factor of 5, while all others are multiplied by a factor of 1.5.

shown in Figure 2. A Gaussian fit to the distribution provides a mean of 6.6 km s^{-1} and a standard deviation of 0.5 km s^{-1}. The spectral resolution of ~45,000 that we obtain is slightly better than that reported on the Keck Web site, but consistent with that value within three times the standard deviation.

3. ANALYSIS

As mentioned in the Introduction, sharp absorptions in the Na I (D) resonance lines of TTSs were noted early on. In 27 out of our 39 targets we find that a similarly sharp absorption is also present in the K I resonance line at 7698.96 Å (see Figures 3–7). We take advantage of the high spectral resolution of HIRES and our large sample of stars covering different evolutionary stages to understand the origin of these sharp features. For each star we calculate the centroid of the absorption and the FWHM and EW of the line (see Tables 5 and 6). We then compare these values to stellar RVs and the velocity and width of low-*J* CO emission lines tracing the cold (~15 K) molecular gas in the Taurus star-forming region.

To compute stellar RVs, we measure the centroid of two prominent photospheric lines that fall in different spectral orders: the Li doublet at a mean wavelength of 6707.83 Å (our spectral resolution is not sufficient to resolve the doublet) and the Ca line at 6439.07 Å. We apply a Monte Carlo approach to evaluate the uncertainty in the peak centroid by adding a normally distributed noise to each spectrum and computing the RV 1000 times for the same star. This uncertainty is typically ~0.2 km s^{-1} except for HN Tau and V410 Tau, for which RV uncertainties are ~3 km s^{-1}; see also Tables 5 and 6. The spectrum of HN Tau has a rather low signal-to-noise ratio (S/N), and the photospheric lines are broad and shallow. Although our RV for HN Tau of 13.8 km s^{-1} is uncertain, it is consistent with the median heliocentric RV of Taurus members, which is 16.2 km s^{-1} (Nguyen et al. 2012). V410 Tau has a stellar companion (see Table 4), and its photospheric lines present multiple components; thus, our fit is sensitive to the wavelength region chosen to fit the line. Two targets HBC 427 and V773 Tau are well-known spectroscopic binaries. For these sources we report the barycenter velocity of the systems calculated from multiepoch spectroscopic campaigns (see Table 6). The standard deviation between the RVs obtained from the Li and Ca lines is ~0.8 km s^{-1}. Most of the stellar

Table 5
2006 Campaign: Heliocentric Radial Velocities, Widths, and EWs of Selected Lines

Source	Stellar[a]	Na			K			^{12}CO	
	RV ($\mathrm{km\ s^{-1}}$)	RV ($\mathrm{km\ s^{-1}}$)	FWHM ($\mathrm{km\ s^{-1}}$)	EW (mÅ)	RV ($\mathrm{km\ s^{-1}}$)	FWHM ($\mathrm{km\ s^{-1}}$)	EW (mÅ)	RV ($\mathrm{km\ s^{-1}}$)	S/N
AA Tau	16.4	17.5	8.8	134	18.1	5.6	73	16.2	28
BP Tau	15.5	13.4	6.0	75	14.5	5.7	22	16.1	15
CW Tau	18.1, 14.8[a]	15.1, 14.7	8.0, 7.7	121, 118	15.4, 14.5	5.4, 5.1	14, 16	15.4	32
CY Tau	17.2	14.1	5.7	71	…	…	…	15.9	63
DF Tau	16.4	15.0	7.5	125	15.4	6.8	99	16.3	27
DG Tau	15.8	14.4	17.8	269	14.5	6.4	86	16.3	20
DK Tau A	15.7	15.6	7.8	146	16.7	7.6	66	16.0	29
DL Tau	14.3	16.0	17.8	275	16.1	6.9	158	15.8	19
DO Tau	17.5	18.0	6.8	106	17.2	6.7	44	16.5	34
DR Tau	21.3	19.9	8.1	127	20.0	5.6	45	21.7	25
GI Tau	17.6	18.0	8.0	131	18.6	5.5	35	16.8	70
GK Tau A	18.2	18.6	7.2	108	19.7	5.2	40	16.8	70
HN Tau A	13.8[b]	19.4	10.1	175	19.9	6.3	75	22.8	0.4
IP Tau	13.9[c]	15.2	6.2	98	15.6	3.9	45	15.8	23
UX Tau A	17.0	20.5	8.5	142	20.3	5.6	39	19.0	13
V819 Tau	16.7	14.0	5.7	72	…	…	…	16.0	37
TW Hya	10.1	…	…	…	…	…	…	…	…

Notes. Sources that have been observed more than once have multiple entries. Stellar RVs have a typical uncertainty of 1 $\mathrm{km\ s^{-1}}$ (see Section 3 for further details). Three dots are used to indicate a nondetection. No entry in the CO columns means that there is no CO map at the location of the source.

[a] This source was observed on two consecutive nights. Note the large change in the Li RV, while the Na I and K I centroids are essentially the same. Throughout the paper we will use 14.8 $\mathrm{km\ s^{-1}}$ as the stellar RV because this value is in agreement with literature values (Hartmann et al. 1986 and Nguyen et al. 2012).

[b] Low-S/N and shallow feature. The reported stellar RV is the mean of 1000 Gaussian fits to the Li line as discussed in Section 3; its uncertainty is 3 $\mathrm{km\ s^{-1}}$.

[c] This source was also observed in our 2012 campaign; the 2012 spectrum has a higher S/N than the 2006 spectrum. Note that both the stellar and the Na I and K I RVs are shifted by ~2 $\mathrm{km\ s^{-1}}$ with respect to the 2012 values (see also Figure 7). This systematic shift suggests a difference in the overall wavelength calibration, maybe as a result of centering the source in the slit. Because the 2012 stellar RV differs by only 0.4 $\mathrm{km\ s^{-1}}$ from that reported in Nguyen et al. (2012), we only use results from the 2012 spectrum in our analysis.

RVs we report in Tables 5 and 6 are from the Li line, except in four instances where this photospheric line appears slightly asymmetric or flat, making it difficult to have an accurate centroid. In these cases, clearly marked in the tables, we use the RV computed from the Ca line at 6439.07 Å. Comparison of our RVs to literature RVs yields differences (excluding the sources with large uncertainties mentioned above) of at most 4 $\mathrm{km\ s^{-1}}$, with the standard deviation being ~1 $\mathrm{km\ s^{-1}}$. Thus, unless specified in Tables 5 and 6, we assign a 1σ uncertainty of 1 $\mathrm{km\ s^{-1}}$ to the stellar RVs reported in this work.

To measure the peak centroid of the molecular gas at the location of our Keck targets, we have used two CO maps of Taurus. One map was obtained with the FCRAO 14 m telescope in the ^{12}CO and ^{13}CO $J = 1$–0 transitions (beam 45″; Narayanan et al. 2008), while the other is a ^{12}CO $J = 1$–0 map acquired with the CfA 1.2 m telescope (beam 8$'$.4; Dame et al. 2001). Ten of our Keck targets[11] lie outside the higher spatial resolution FCRAO map but are covered by the coarser CfA ^{12}CO map. For all targets we extract the ^{12}CO and the ^{13}CO spectra at the source location and compute the centroid velocity over a ~6 $\mathrm{km\ s^{-1}}$ window centered around the Taurus mean velocity, ~6 $\mathrm{km\ s^{-1}}$ LSR (e.g., Goldsmith et al. 2008), the uncertainty in the centroid, and the S/N of the CO spectrum. The ^{12}CO and ^{13}CO centroids from the FCRAO map are very similar, their standard deviation being only 0.2 $\mathrm{km\ s^{-1}}$, but the ^{12}CO profiles are broader (typical full width at half maximum of ~1.5 $\mathrm{km\ s^{-1}}$; see also Goldsmith et al. 2008). For spectra with an S/N greater than 5 and sources in common in the FCRAO and CfA surveys we find that the standard deviation in the peak centroids is ~0.4 $\mathrm{km\ s^{-1}}$, and there are no cases for which the absolute difference in the centroids is larger than 1 $\mathrm{km\ s^{-1}}$. Given that the uncertainty in the RVs obtained from the optical spectra is ~1 $\mathrm{km\ s^{-1}}$, we have opted to provide the peak centroids and the S/N of the CO spectra extracted from the CfA Taurus map that covers all of our targets (see Tables 5 and 6).

3.1. Residual Na I and K I Profiles

A comparison of residual Na I and K I resonance profiles and Li photospheric lines is shown in Figures 3–7. Because K I absorption lines are on average a factor of ~2 weaker than Na I lines, we have scaled these profiles when needed; scaling factors are provided in the figure captions. In all objects except TW Hya and perhaps V1348 Tau (Figure 6) it is possible to identify one absorption feature in the Na I profile that is narrower than the photospheric Li line and is close to, but not always coincident with, the stellar RV. Similar narrow absorptions are present in the K I profiles of about two-thirds of the targets.

Five sources (DO Tau, CI Tau, HQ Tau, IT Tau, and V836 Tau) present one additional narrow absorption that is more offset from the stellar RV (see Figure 8). Except for CI Tau and HQ Tau, this extra absorption is only clearly detected in the Na I profiles. For IT Tau the additional absorption is at $v_{\mathrm{helio}} \sim -2\ \mathrm{km\ s^{-1}}$, about 18 $\mathrm{km\ s^{-1}}$ blueshifted from the

---

[11] The targets that are not covered by the FCRAO map are DR Tau, HN Tau, UX Tau, DM Tau, GM Aur, HBC 427, V710 Tau, V836 Tau, V1321 Tau, and V1348 Tau.

Table 6
2012 Campaign: Heliocentric Radial Velocities, Widths, and EWs of Selected Lines

Source	Stellar[a]	Na			K			^{12}CO	
	RV (km s^{-1})	RV (km s^{-1})	FWHM (km s^{-1})	EW (mÅ)	RV (km s^{-1})	FWHM (km s^{-1})	EW (mÅ)	RV (km s^{-1})	S/N
Anon 1	16.3	16.1	10.7	110	…	…	…	15.4	57
CI Tau	19.1[b]	19.1	11.3	218	17.4, 23.4	6.1, 6.1	60	16.5	27
CoKu Tau4	17.9, 17.1	16.3, 15.5	7.4, 7.5	128, 121	16.3, 15.3	5.7, 5.0	52, 49	15.1	17
DH Tau	16.4	17.8	7.6	114	17.4	5.6	45	16.0	37
DM Tau	18.5*	21.5	6.8	90	…	…	…	21.8	1.4
DN Tau	17.6*	18.1	9.1	142	…	…	…	16.6	44
DS Tau A	16.2	15.6	5.8	72	…	…	…	16.0	11
FM Tau	16.0	15.6	7.1	83	15.0	3.2	4	15.4	32
FZ Tau	18.0, 18.1	19.8, 19.9	8.4, 8.7	140, 138	20.4, 20.6	5.9, 6.7	81, 89	16.4	83
GH Tau	18.4	19.6	7.5	111	20.2	5.1	42	16.5	35
GM Aur	15.6	16.2	7.0	87	…	…	…	14.2	2.2
GO Tau	17.2, 17.5	18.1, 18.3	6.7, 6.0	106, 86	…	…	…	16.6	28
HBC 427	14.35[c]	16.2	7.1	123	…	…	…	14.7	4.9
HQ Tau	17.1	19.1	9.9	169	18.7, 27.3	7.9, 9.2	197	17.2	15
IP Tau	16.1	17.3	6.8	86	17.7	5.6	30	15.8	23
IT Tau A	16.1	17.5	8.5	146	17.2	8.5	95	15.4	30
UX Tau A	16.5	20.7	8.3	150	19.9	5.4	36	19.0	13
VY Tau	17.1	20.9	7.8	119	…	…	…	16.0	1.7
V410 Tau	16.0[d]	14.6	8.1	117	14.0	5.0	4	16.1	74
V710 Tau A	20.0	21.4	8.3	126	23.0	5.4	32	18.8	28
V773 Tau	16.4[c]	15.6	9.4	146	16.0	7.4	34	15.3	34
V836 Tau	19.2*	20.1	5.6	57	18.8	5.7	31	18.1	13
V1321 Tau	21.3	22.1	7.5	133	22.7	3.1	12	21.5	1.9
V1348 Tau	15.4*	22.9(?)	8.4(?)	…	…	…	…	24.0	1.6

Notes. Sources that have been observed more than once have multiple entries for the RV and FWHM. The reported optical RVs have a typical uncertainty of 1 km s^{-1}, while CO RVs have 0.2 km s^{-1} (see Section 3 for further details). Two components are present in the K I absorption line toward CI Tau and HQ Tau (see Figure 8); hence, we fit these profiles with the sum of two Gaussian curves.

[a] The symbol * indicates that the stellar RV is computed from the Ca line (6439.07 Å) instead of being computed from the Li line.

[b] Suspected spectroscopic binary (Nguyen et al. 2012).

[c] Known spectroscopic binaries. We report and use the velocity of the barycenter of the systems as in Steffen et al. (2001) for HBC 427 and Rivera et al. (2015) for V773 Tau.

[d] Two components are visible in the Li line. The single Gaussian fit we perform here is sensitive to how much of the continuum is included in the fit. The reported stellar RV is the mean of 1000 Gaussian fits to the Li line, as discussed in Section 3; its uncertainty is 3 km s^{-1}.

stellar RV, while for DO Tau and V836 Tau it is at ~7.3 km s^{-1}, 10 and 12 km s^{-1} blueshifted from the stellar RV. CI Tau and HQ Tau are at a projected distance of only 0.5 degrees from each other, and both present extra absorption at higher velocities, specifically at 23.4 and 27.3 km s^{-1}, respectively. This implies that the absorption is redshifted by 4.3 and 10.2 km s^{-1} from the stellar RV.

As previously reported in the literature, Na I profiles of TTSs present a range of morphologies. More than half of our sample stars (23/39) show Na I emission, with the highest accretors having FWHMs clearly broader than photospheric lines (see, e.g., CY Tau and DO Tau in Figure 3). Magnetospheric infall is the most likely origin of this emission, but stellar winds may also contribute. Conversely, the Na I emission of WTTSs is similar in width to (or narrower than) photospheric lines (see Figure 6). While some of this excess emission may result from an improper photospheric subtraction (see Section 2 for details), the stellar chromosphere may also contribute. Broad absorptions in the Na I profiles that are clearly outside the range of photospheric velocities are detected toward five stars (DF Tau, DG Ta, DL Tau, DO Tau, and DR Tau; see Figure 14). The restricted velocity range adopted in Figures 3–5 only shows the blueshifted component of the broad absorption, which is associated with ejected material. However, in all cases there is also redshifted Na absorption that traces infalling disk gas onto the star (see appendix). We note that for all of the sources in our sample, K I profiles are less complex than Na I profiles. This is evident both in the sample of high accretors ($\dot{M} \geqslant 10^{-8}\,M_\odot$ yr^{-1}; only DG Tau and DO Tau have a broad blueshifted K I absorption beyond the photospheric line) and in the sample of low/no accretors (see, e.g., the presence of only one absorption line in the K I residual profiles of IT Tau and V773 Tau). In the next sections, we will discuss the origin of the narrow Na and K absorptions, excluding the second components seen in five stars with velocities differing significantly from the stellar velocity.

3.2. Empirical Trends

In this section we present empirical trends between the narrow and sharp Na I and K I absorption features, extinction along the line of sight, stellar RVs, and the velocity of the cold molecular gas in Taurus.

As mentioned earlier, a deep narrow Na I absorption is present in all spectra except those of V1348 Tau and TW Hya, while K I absorption is present in two-thirds of the spectra. With perhaps the exception of V836 Tau, the Na I lines appear highly saturated; hence, their EWs cannot be used to infer the

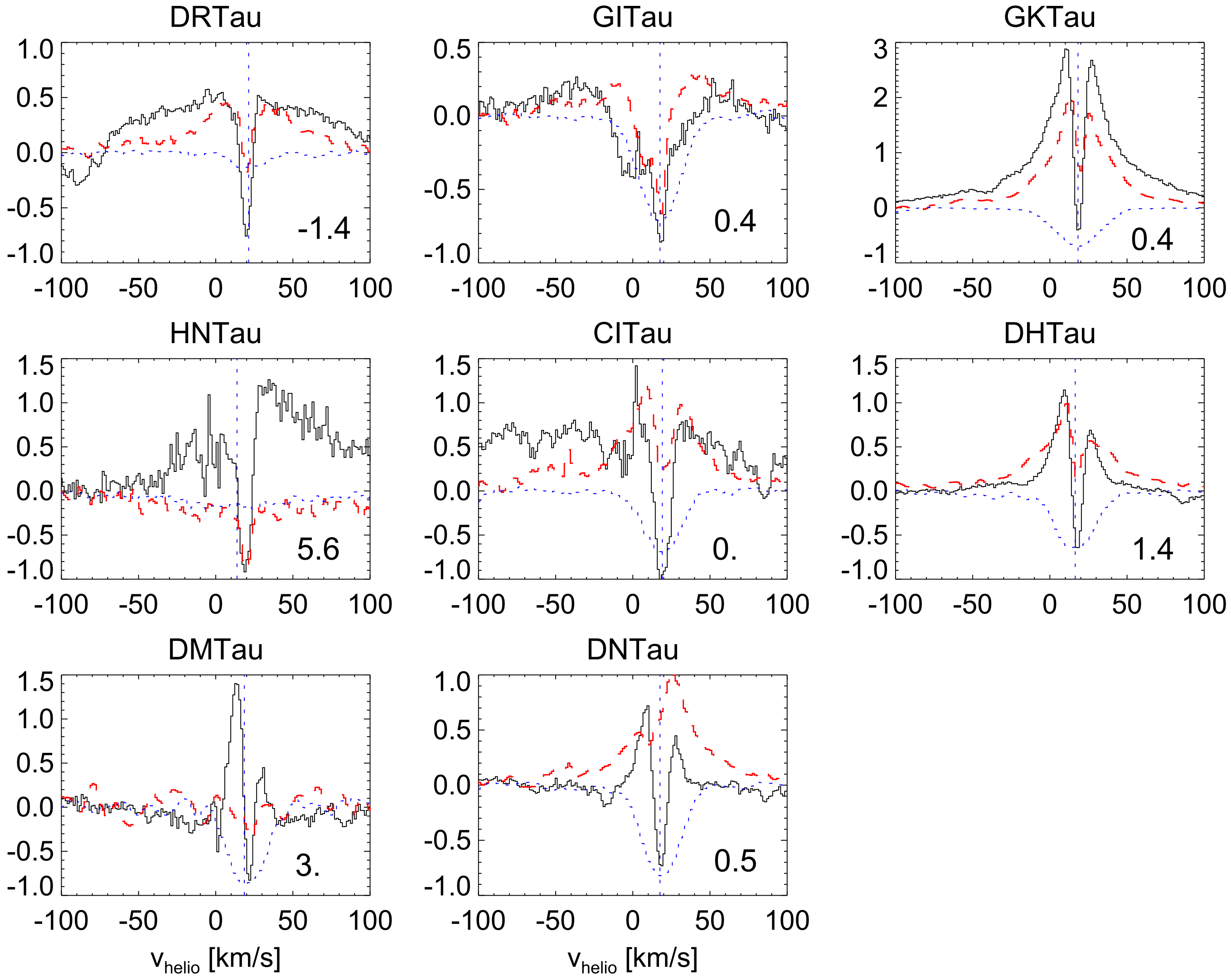

Figure 4. Same as Figure 3. All K i profiles are multiplied by a factor of 2.

column density of the absorbing material. Saturation is also common in the K i lines when detected. For both transitions, line FWHMs span a larger range of values (by a factor of ~3) than RVs and are not correlated with them. When absorptions are present in both the Na i and K i profiles, their RVs are the same within our ~1 km s^{-1} velocity accuracy, the median absolute value of their difference being 0.6 km s^{-1}. This is illustrated in the upper left panel of Figure 9, where a linear fit to the centroids of the Na i and K i absorptions results in a slope very close to unity. Although the EWs of the absorption lines are more sensitive to the photospheric subtraction than peak centroids, and hence less accurate, the Na i and K i EWs are correlated. The Kendall τ test (see, e.g., Press et al. 1993, p. 77) on the subset of sources with detections in both lines returns $\tau = 0.4$ and a probability of 5×10^{-4} that the variables are uncorrelated. These results demonstrate that there is a significant positive correlation between the Na i and K i EWs, with the K i absorption, when detected, being a factor of ~2 lower than the Na i absorption (Figure 9, upper right panel). The fact that Na and K sharp absorptions occur at the same heliocentric RV and their EWs are positively correlated strongly suggests that the two atomic transitions trace the same gas. One notable difference in their absorption profiles is the line width: many Na i absorption lines are spectrally resolved (the mean FWHM is 8.2 km s^{-1}), while most K i lines are unresolved with a mean FWHM of 6.3 km s^{-1}, the same as that measured for telluric lines. We will discuss this further in Section 4.

We also test whether there is any correlation between the optical extinction along the line of sight (A_V) and the Na i and K i EWs, line-to-continuum ratios,[12] and RVs. It is known that extinctions are rather uncertain and depend on the specific technique and wavelength range used to derive them (see, e.g., discussion in Edwards et al. 2013; McJunkin et al. 2014). Recently, Herczeg & Hillenbrand (2014) have recomputed spectral types, extinctions, and accretion in a homogeneous way for over 280 nearby TTSs using an improved technique that fits simultaneously these three parameters to flux-calibrated optical spectra. All but four of our sources overlap with their sample; hence, we use this homogenous set of A_V for our analysis. In spite of a relatively large scatter, which may be due to our use of photospheric templates to compute the residual profiles of these gravity-sensitive lines, the Kendall τ test

---

[12] The line-to-continuum ratio is defined here as the depth of the absorption line with respect to the local continuum.

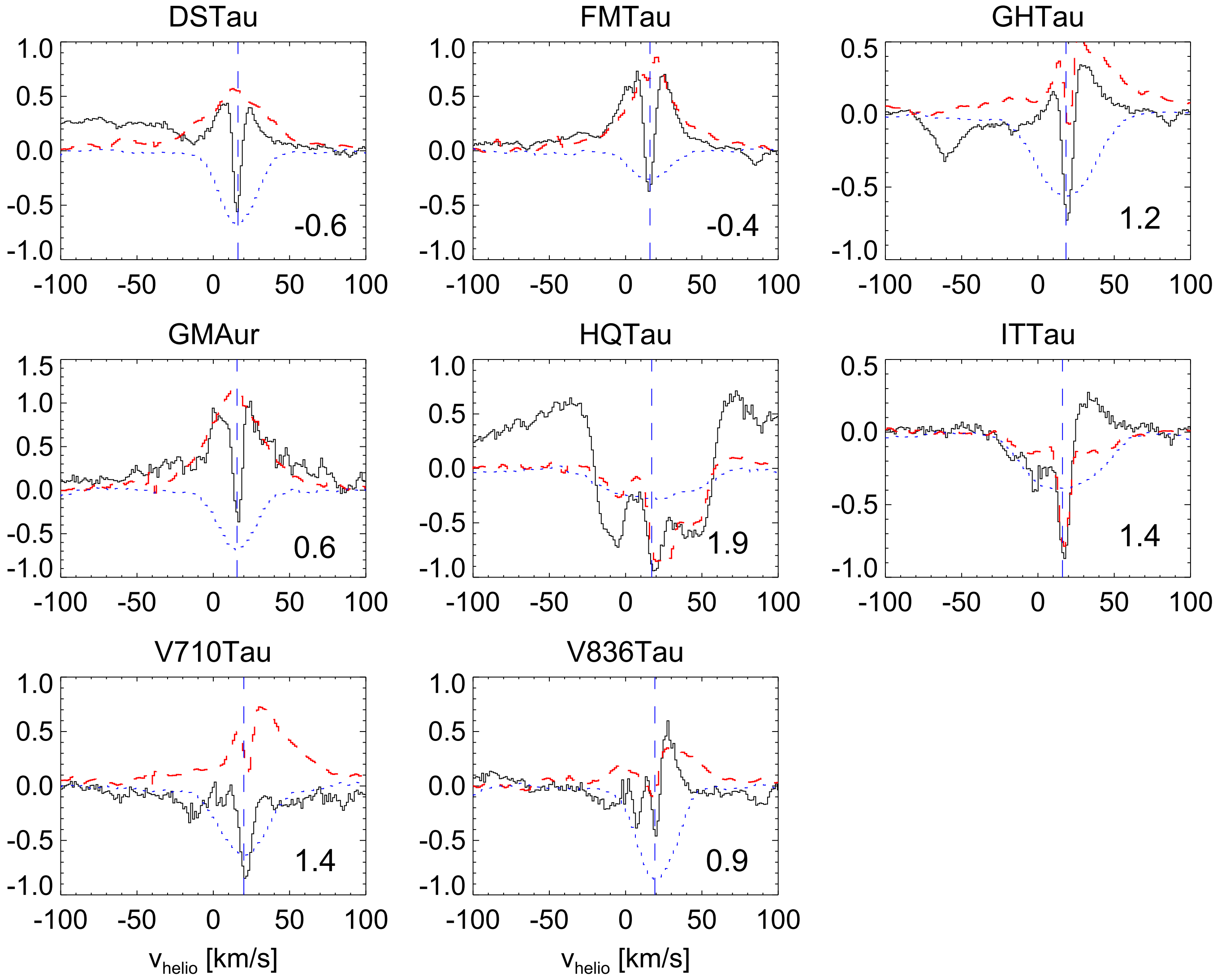

Figure 5. Same as Figure 3. All K i profiles are multiplied by a factor of 1.5.

suggests a moderate positive correlation between the line EWs and A_V, $\tau = 0.4$, and a lower probability that the variables are uncorrelated for Na (5×10^{-3}) than for K (7×10^{-2}) (see also Figure 9, lower left panel). The Na i line-to-continuum ratios are less correlated with A_V, but a modest correlation remains between the K i line-to-continuum ratios and A_V, $\tau = 0.4$, and probability of being uncorrelated of 2×10^{-2} (Figure 9, lower right panel). Finally, the RVs of the Na i lines are not correlated with A_V ($\tau = 0.01$ and probability of 0.9). These results hint to a possible relation between the gas probed via the Na and K absorption lines and the location of our targets in the Taurus molecular cloud.

We now turn to the comparison between the RVs of the Na and K absorption features and the stellar RVs provided in Tables 5 and 6. A histogram of the difference between these quantities is shown in Figure 10. According to the nonparametric Kolmogorov–Smirnov (K-S) statistics, there is a ~12% probability that the two velocity distributions are drawn from the same parent population, in other words, they are statistically indistinguishable. Indeed, for many sources the Na and Li RVs are the same given our velocity uncertainty. However, there are sources for which the absorption lines are clearly redshifted (e.g., VY Tau, DM Tau, UX Tau A) or blueshifted (e.g., BP Tau, CY Tau, V819 Tau) with respect to the stellar RV; see Figures 3–7. This group comprises CTTSs and WTTSs, Class II and III SEDs, as well as transition disks (TDs). One thing in common to these sources with deviant velocities is that they lie at the edge of the Taurus molecular cloud; see Section 4. Thus, atomic Na and K gas is not always associated with the immediate circumstellar environment.

In further comparing the stellar and Na i RVs with the velocity of the molecular gas, we restrict ourselves to CO spectra with an S/N greater than 5, thus excluding HN Tau, DM Tau, HBC 427, GM Aur, VY Tau, V1321 Tau, and V1348 Tau. As already reported in the literature (e.g., Hartmann et al. 1986), we do not find any statistically significant difference between the stellar RVs and the RVs of the molecular CO gas at the source location (K-S probability ~12%; see also Figure 10). This is expected because stars form in molecular clouds, thus inheriting the cloud velocity field, and clouds are not dispersed in ~1–2 Myr. Interestingly, the distributions of RVs for the atomic and molecular components are statistically different, with a K-S probability of only 0.6% that they are drawn from the same parent population; see also

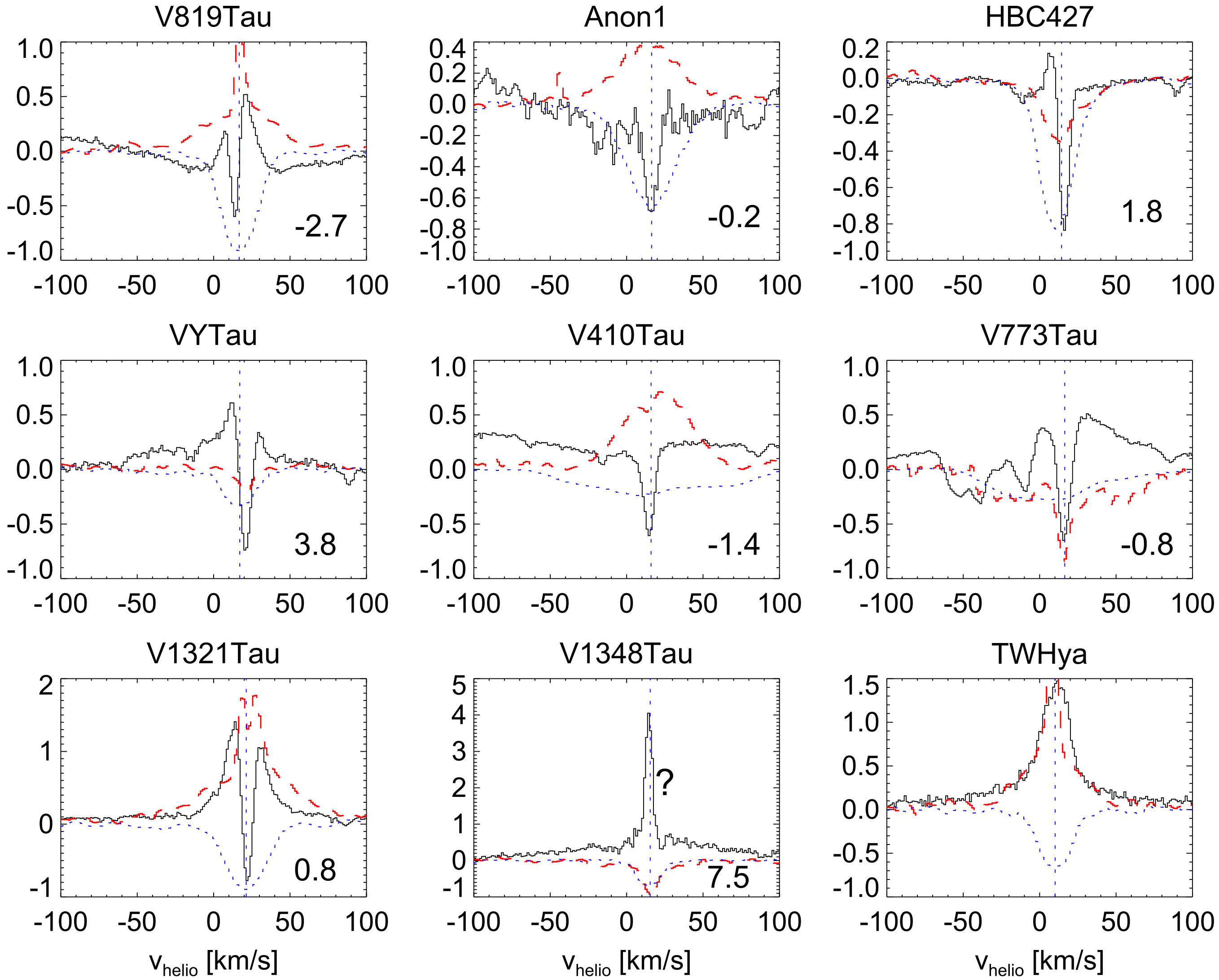

Figure 6. Same as Figure 3 but for the sample of WTTSs and TW Hya. The K i profiles of V410 Tau and V1321 Tau are multiplied by a factor of 2, while that of V773 Tau by a factor of 5.

Figure 10. This strongly suggests that the molecular gas and atomic gas are not co-located. Sources with low-S/N CO detections but strong Na i absorption, such as VY Tau and DM Tau, further strengthen this statement (see Figure 6) and suggest that the atomic gas is more extended than the molecular gas. We also note that the FWHMs of the ^{12}CO lines are much narrower than those of the Na i lines and would all appear unresolved at the resolution of our optical spectra. However, this difference in FWHMs may be due to a combination of saturation of the Na i lines and the presence of other atomic clouds along the line of sight; hence, it does not further constrain the spatial location of the molecular and atomic gas.

To summarize, we find that (i) Na i and K i absorption lines trace the same atomic gas, but Na i profiles are often spectrally resolved while K i lines are not; (ii) there is a modest correlation between the EW of these absorption features and A_V; and (iii) although there is no statistical difference between the stellar RV distribution and either the Na i or CO RVs, the RVs of the atomic gas and molecular gas are unlikely to be drawn from the same parent population.

4. ORIGIN OF THE NARROW ABSORPTION IN THE NA i AND K i PROFILES

Previous studies of Na absorption lines could not distinguish between a disk and an interstellar/cloud origin because they investigated fewer stars, mostly CTTSs with Class II SEDs, at a lower spectral resolution than achieved here. By extending our sample to include WTTSs and Class III SEDs and with a precision in RV of ~ 1 km s^{-1}, we can exclude that the sharp and narrow Na i and K i absorption lines trace circumstellar disk gas. There are three main observables pointing against a disk origin. First, strong absorption features are also detected toward objects that are not surrounded by disks (e.g., Anon 1) or have only tenuous dust disks more akin to debris disks (e.g., V1321 Tau). Second, if the absorbing material were disk gas, there should be only one narrow absorption feature toward single stars, and its velocity should be coincident with the stellar RV. As discussed in the previous subsection, this is not the case for several systems. Third, as will be shown later in this section, there is a spatial gradient in the RV of the Na i lines indicating a location in the distributed gas rather than the immediate circumstellar environment.

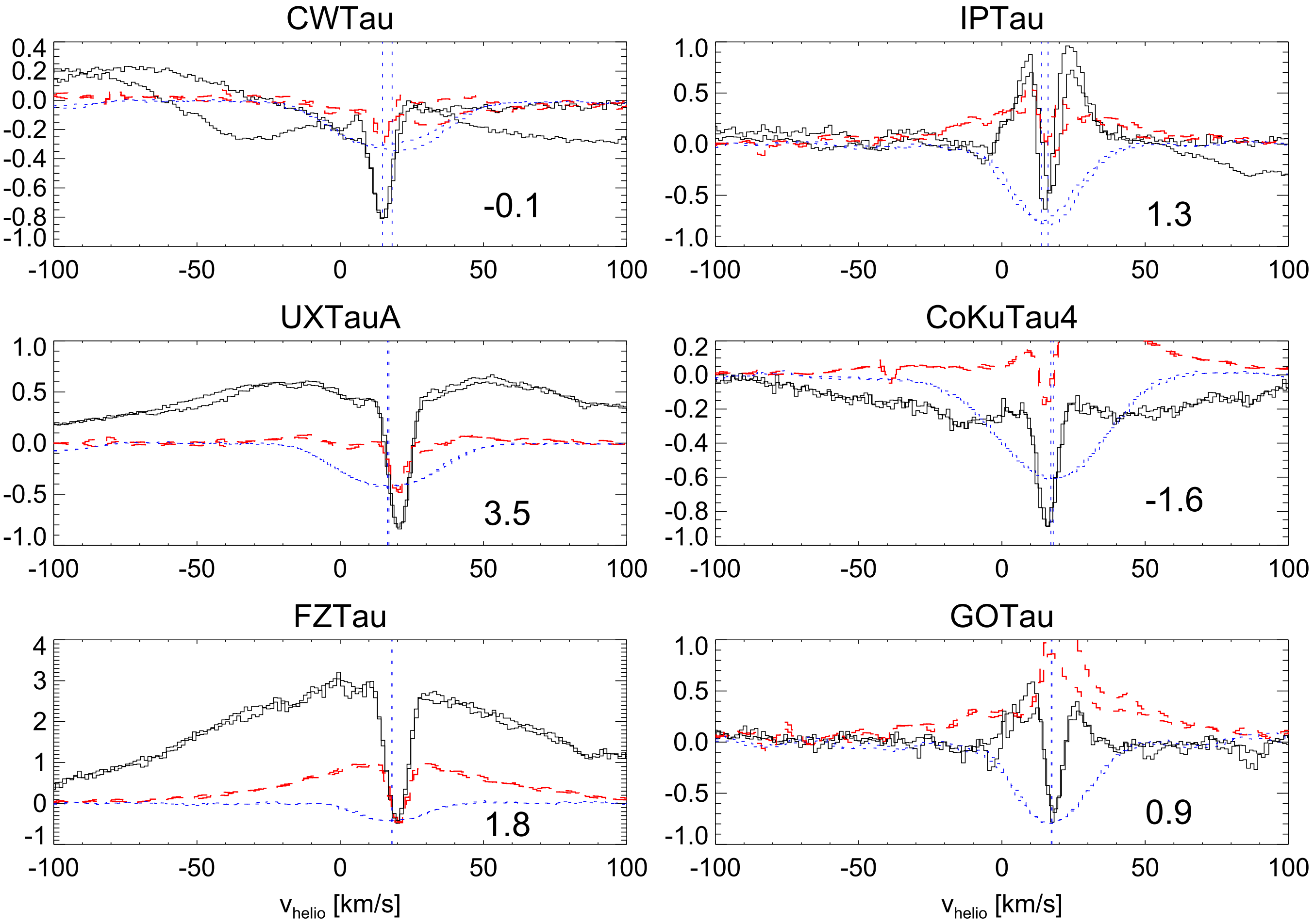

Figure 7. Same as Figure 3 but for sources that have multiple observations. The K I profiles of CoKu Tau4 are multiplied by a factor of 2. The sharp absorptions in the Na I and K I are not time variable. Note that the IP Tau 2006 Na I and the Li heliocentric velocities are both ∼1.8 km s^{-1} smaller than in the 2012 spectra, while the difference between the Na I and Li lines remains the same in the two epochs. This shows that the absolute wavelength calibration can be off by up to ∼2 km s^{-1}, perhaps depending on the source centering, as found in the comparison between our and literature RVs (Section 3).

Redfield & Linsky (2008) constructed an empirical dynamical model of the local ISM (inside the Local Bubble, i.e., within about 100 pc) using UV *Hubble Space Telescope* spectroscopy toward 157 sight lines. While their model relies on the more numerous Ca II absorption lines, they find that all Na I absorption components have companion Ca II absorption at the same velocity. This indicates that the gas detected by the Ca II absorption is physically associated with that detected with the Na I line. Nine of their stars are in the direction of the Auriga cloud. We use the cloud heliocentric velocity vectors they derive (their Table 16) to compute the RV of the Local Bubble gas at the location of each of our targets. With a mean predicted RV of 20 km s^{-1} and minimum and maximum of 19 and 23 km s^{-1}, respectively, the gas in the Local Bubble cannot be responsible for the average Na I RV of 17.6 km s^{-1} and the larger range of velocities (from ∼13 to 23 km s^{-1}) we find in our sample. Only 13 out of 38 unique Keck targets have RVs consistent with those predicted by the Local Bubble model of Redfield & Linsky (2008), and the K-S test gives a probability of only 3×10^{-8} that the two velocity distributions are drawn from the same parent population. In addition, of the nine stars in the direction of the Auriga cloud, only one of them has a detected Na I absorption component with an EW of only ∼3 mÅ (Farhang et al. 2015), much smaller than the absorption we measure toward our TTSs. We conclude that the Na I and K I absorption features we detect are not associated with Local Bubble gas. This conclusion is also consistent with the lack of absorption in the Na I and K I profiles of TW Hya, which is at only ∼50 pc from the Sun (Mamajek 2005), albeit in a different direction from Taurus.

The distribution of interstellar gas and its kinematic beyond the Local Bubble is less well established. Welty & Hobbs (2001) obtained high-resolution (FWHM ∼ 0.4–1.8 km s^{-1}) spectra of K I absorption toward 54 Galactic OBA stars. One of them, HD 27778 (62 Tau), is in the direction of the Taurus star-forming region at a projected separation of ∼1°.5 from DF Tau and ∼1°.9 from DG Tau and FZ Tau. At a distance of 225 pc, as measured by *Hipparcos* (ESA 1997), HD 27778 is not a Taurus member but likely belongs to the older Cas-Tau OB association located behind the Taurus molecular cloud (e.g., Mooley et al. 2013). The K I profile obtained by Welty & Hobbs (2001) shows two deep and spectrally resolved absorptions at ∼14.8 km s^{-1} (consistent with the DF Tau and DG Tau Na I and K I velocities) and ∼18.5 km s^{-1} (slightly lower than the FZ Tau velocities). The Na I absorption profile along the same line of sight is highly saturated (see their Figure 2), because sodium is ∼15 times more abundant than potassium. This means that the identification of individual clouds is more challenging using Na I lines even at high spectral resolution. Saturation and blending of clouds at similar velocities might explain why many Na I absorption lines toward the Taurus TTSs are resolved at our spectral resolution, ∼4 times

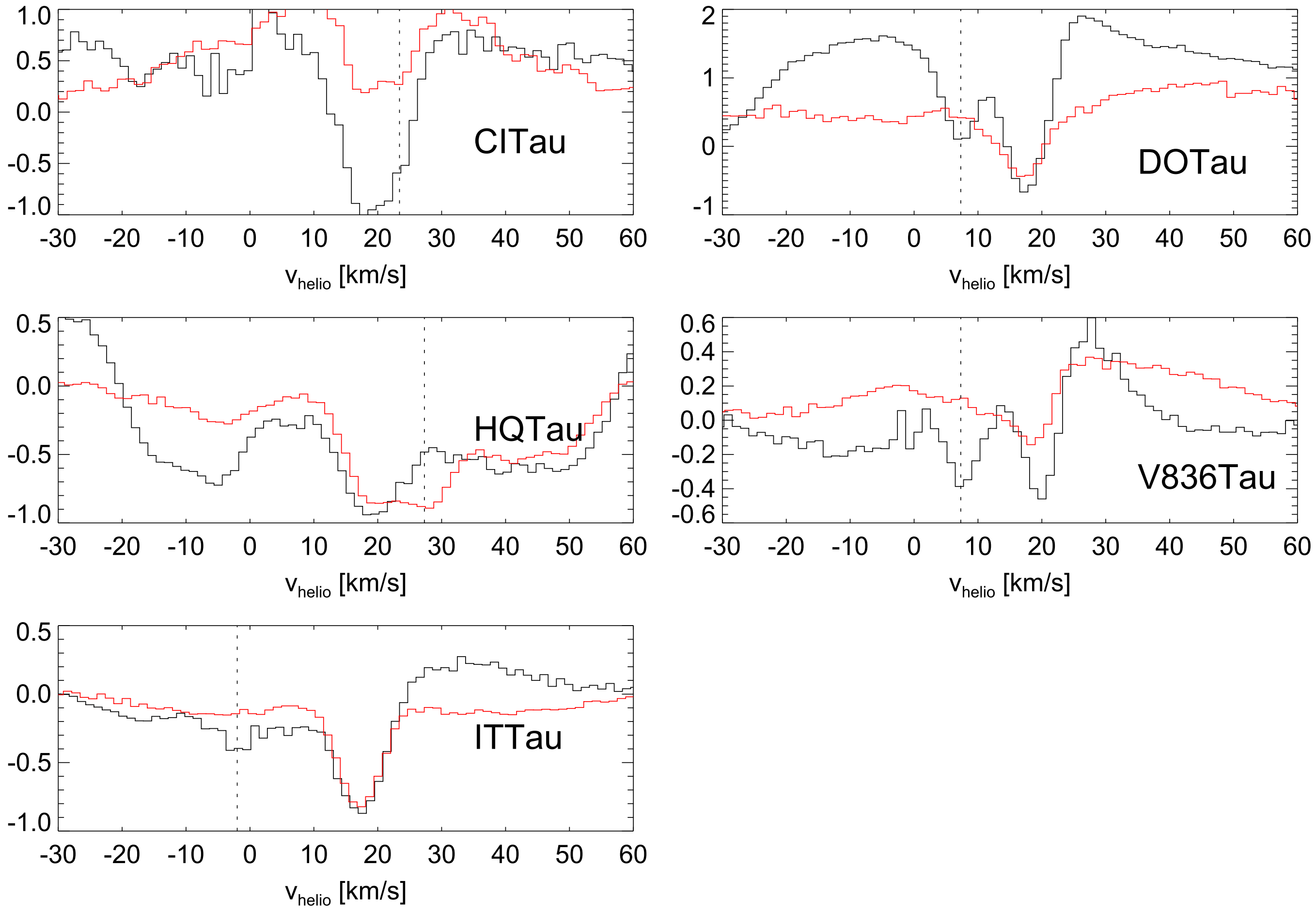

Figure 8. Comparison of Na I (black) and K I (red) residual profiles for the five TTSs showing one additional narrow absorption feature in their spectra. As in previous figures, the K I profiles are multiplied by a factor of 5 for DO Tau, a factor of 2 for CI Tau, and a factor of 1.5 for the other three sources. The location of the additional narrow component is indicated with a dotted line. We do not include these additional narrow components in any of our analyses.

lower than that of Welty & Hobbs (2001), while most K I lines remain unresolved. As pointed out in Section 3.2, this is clearly the case for HQ Tau and CI Tau, where two cloud components are detected in the K I but remain blended in the Na I profiles. Welty & Hobbs (2001) model the K I profile observed toward HD 27778 with six atomic clouds in the foregrounds; four of them have RVs within 2 km s^{-1} of the median stellar RVs of Taurus members. For these clouds they estimate K I column densities between 1.4×10^{11} and 1.9×10^{11} cm^{-2}, which correspond to an average $\sim 6 \times 10^{20}$ cm^{-2} hydrogen column given their empirical relation between K and H column densities. As a comparison, McJunkin et al. (2014) find H column densities of $\sim(2.5\text{–}10) \times 10^{20}$ cm^{-2} toward 12 TTSs in Taurus from neutral hydrogen absorption against broad Lyα emission profiles. These column densities are consistent with each other, about two orders of magnitude larger than the H column densities measured inside the Local Bubble (Redfield & Linsky 2008), but rather typical to ISM clouds (Welty & Hobbs 2001).

Do the Na I and K I narrow absorption features trace atomic gas associated with the Taurus molecular cloud or rather ISM gas beyond the Local Bubble? To answer this question, we plot the location of our TTSs on the sky and color-code the RV of the absorbing material toward them (see Figure 11).[13] The figure reveals that nearby sources have similar velocities and a clear spatial gradient in RVs with lower RVs NW and higher RVs SE. Several authors have argued that linear velocity gradients in giant molecular clouds are the result of large-scale cloud rotation (e.g., Blitz 1993, p. 125). Following common practice and assuming solid-body rotation (e.g., Goodman et al. 1993), we fit a plane to identify the best-fit linear velocity gradient and measure its magnitude (Ω) and direction (θ), i.e., the direction of increasing velocity measured east of north. The rotation axis of the cloud is then $\theta + 90°$. With this approach we find that $\theta \sim 125°$ (P.A. of the rotation axis 215°),[14] which is the same as Galactic rotation, $\Omega \sim 0.11$ km s^{-1} pc^{-1}, and the mean LSR cloud velocity is 7.2 km s^{-1}. To demonstrate that a plane is a good fit to the velocity map, we show in Figure 12 a position–velocity diagram passing through the center of the CO map, where the position is the offset of each star along the direction perpendicular to the rotation axis. As expected for gas rotating as a solid body, we see a linear trend in the velocity as a function of offset from the rotation axis. Thus, it appears that the atomic gas associated with the Taurus molecular cloud rotates in the same direction of Galactic rotation (Kleiner & Dickman 1985). Evidence for global rotation of the Taurus complex has been recently reported by Rivera et al. (2015) from the RVs and

---

[13] We use the RV of the Na I lines because we have more detections in this line than in the K I line and have already demonstrated that when both lines are detected there is a good coincidence between their RVs.

[14] These values are obtained including V1348 Tau. If we exclude this source, we find P.A. = 214° and $\Omega = 0.11$ km s^{-1} pc^{-1}, basically the same as those reported in the text.

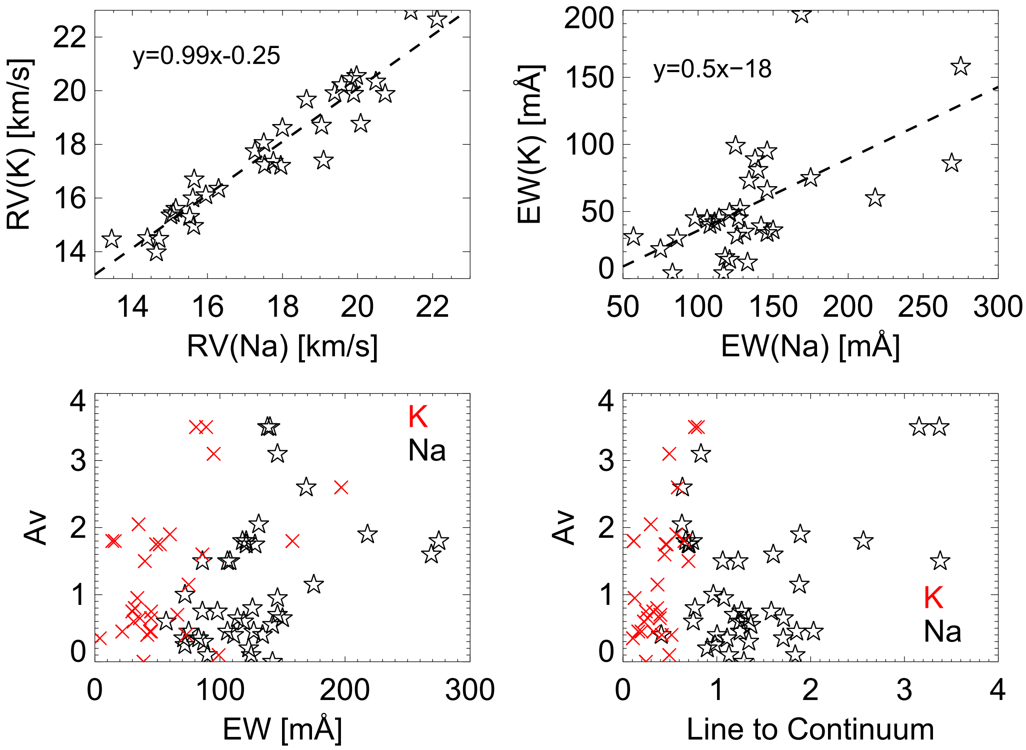

Figure 9. Upper panels: comparison of Na I and K I peak centroids (left) and EWs (right). We only plot sources where both narrow absorption lines are detected. Both quantities are positively correlated. In both panels a dashed line shows the best linear fit. Lower panels: source extinction A_V as a function of EW (left) and line-to-continuum ratio (right). Detected Na I absorptions are shown with stars, while K I absorptions with crosses. The EWs of Na I lines are about 2 times larger than those of K I lines.

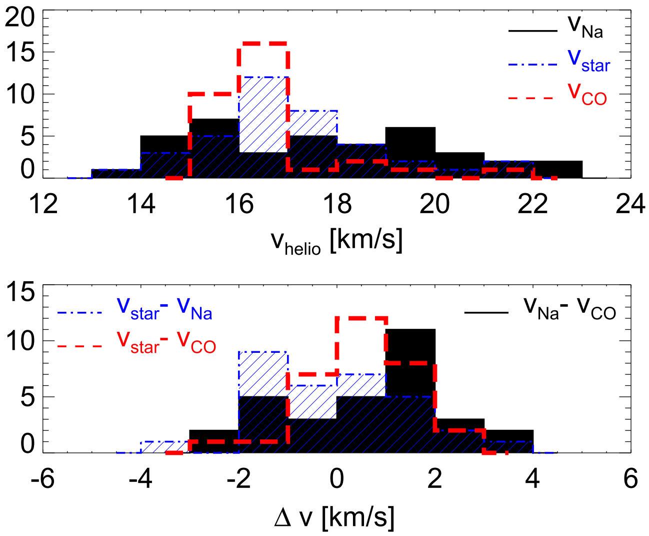

Figure 10. Distribution of heliocentric RVs (upper panel) and velocity differences (lower panel). For the molecular gas we only include sources for which the S/N of the ^{12}CO spectra is larger than 5 (see last column of Tables 5 and 6).

proper-motion measurements for seven well-known Taurus members. These authors find velocity gradients of $\sim$0.1 km s^{-1} pc^{-1} and positive direction of rotation with respect to Galactic rotation, as we find from the study of the Na I lines.

Velocity gradients in Taurus have also been measured using other tracers, and it has long been known that the Taurus velocity field is rather complex even on large $\sim$10 pc scales (e.g., Shuter et al. 1987). Here we are particularly interested in comparing the atomic and the molecular components. Figure 13

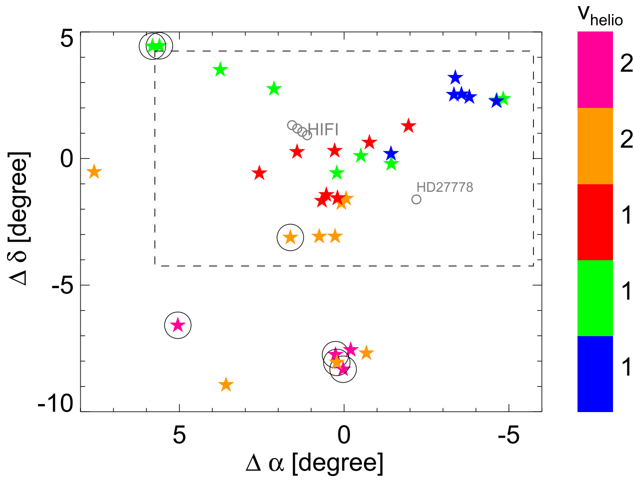

Figure 11. Distribution of our TTSs (stars) in relative equatorial coordinates. The center of the plot is the center of the CO map (Narayanan et al. 2008); its extent is shown by the dashed rectangle. TTSs are color-coded based on their Na I heliocentric RVs: each color bin covers 2 km s^{-1}, and the mean RV for each color bin is listed next to the color bar. We also plot the location of the background B3 star HD 27778 studied by Welty & Hobbs (2001) and of the *Herschel*/HIFI pointings by Orr et al. (2014). The S/N of the ^{12}CO CfA spectra toward circled stars is less than 5. As mentioned in the text and Figure 6, the detection of Na I absorption toward V1348 Tau is not secure. Note that the Na I RVs increase going from NW to SE.

shows the Na I velocities (as stars) superimposed on the higher spatial resolution ^{13}CO FCRAO map.[15] The ^{13}CO gas shows an SE–NW gradient with a rotation axis of 25°, $\Omega \sim$ 0.25 km s^{-1} pc^{-1}, and a systemic LSR velocity of 6.4 km s^{-1}

---

[15] We use the FCRAO map because it has higher spatial resolution and only four sources are detected beyond this map in the coarser CfA survey.

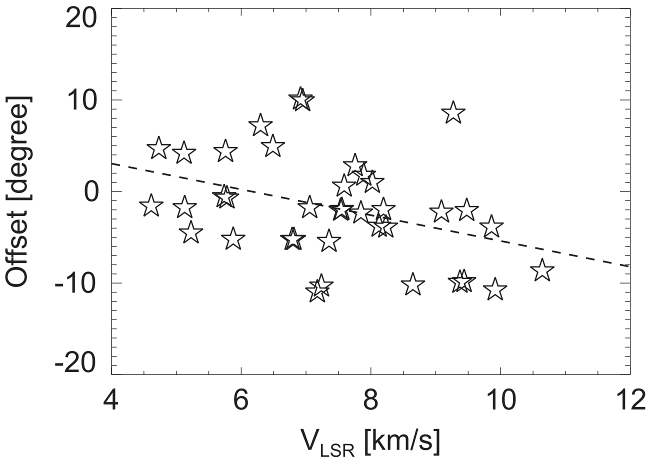

Figure 12. Perpendicular offset of each TTS from the Na cloud rotation axis (P.A. = 210°) as a function of the Na I LSR velocity. The linear trend between the two quantities shows that a plane is a good fit to the velocities.

(Shuter et al. 1987). The ^{13}CO rotation is almost antiparallel to that of the Na I gas and retrograde with respect to differential galactic rotation. Interestingly, Ballesteros-Paredes et al. (1999) find that the H I 21 cm emission has also a velocity offsets of a few kilometers per second and a larger velocity dispersion ($\sim$5–10 km s^{-1} LSR) than the molecular CO gas, resembling the one we see in the Na I and K I absorption lines. Position–velocity diagrams along some directions show a different axis of rotation from the CO gas (e.g., Figure 3(a) of Ballesteros-Paredes et al. 1999), but the magnitude and direction of rotation of the H I emitting gas have not been quantified. As a note, the magnetic field in Taurus has a mean P.A. of 25° (=205°), the same as the CO and Na I rotation axes. This is consistent with the classic theory of isolated low-mass star formation, whereby cores contract more along magnetic fields, resulting in a rotating flattened morphology perpendicular to the field axis (e.g., Shu et al. 1987). What is surprising is that the atomic gas and molecular gas rotate in almost opposite directions. What is the relation between the atomic and molecular gas?

The larger velocity dispersion in the Na I and K I absorptions and in the H I 21 cm emission compared to the CO peak velocities suggests that the atomic gas is more widely distributed. Indeed, these atomic tracers are detected even at locations where molecular CO gas is not detected. Thus, they appear to trace the atomic gas that is the leftover of star formation. In addition, the mere detection of alkali metals in the gas phase implies that there are regions warmer than those traced by CO, regions that are not shielded from the ambient FUV radiation, or else Na and K would be depleted onto the surface of dust grains (e.g., Barlow 1978). We can further place an upper limit on the gas temperature that would result in thermal broadening (for the moment we neglect turbulence) by assuming that each atomic cloud is spectrally unresolved at our 6.6 km s^{-1} resolution (such as, for instance, toward BP Tau or V819 Tau). Sodium gives a more stringent constraint than potassium, given its lower atomic mass, but not a tight one: the gas temperature should be $\leqslant$2000 K for sodium lines to be unresolved at our spectral resolution. A much tighter constraint comes from the higher-resolution spectra of Welty & Hobbs (2001). These authors measure K I line width parameters ($b \sim$ 1.667 FWHM) for over 100 ISM clouds, including those in

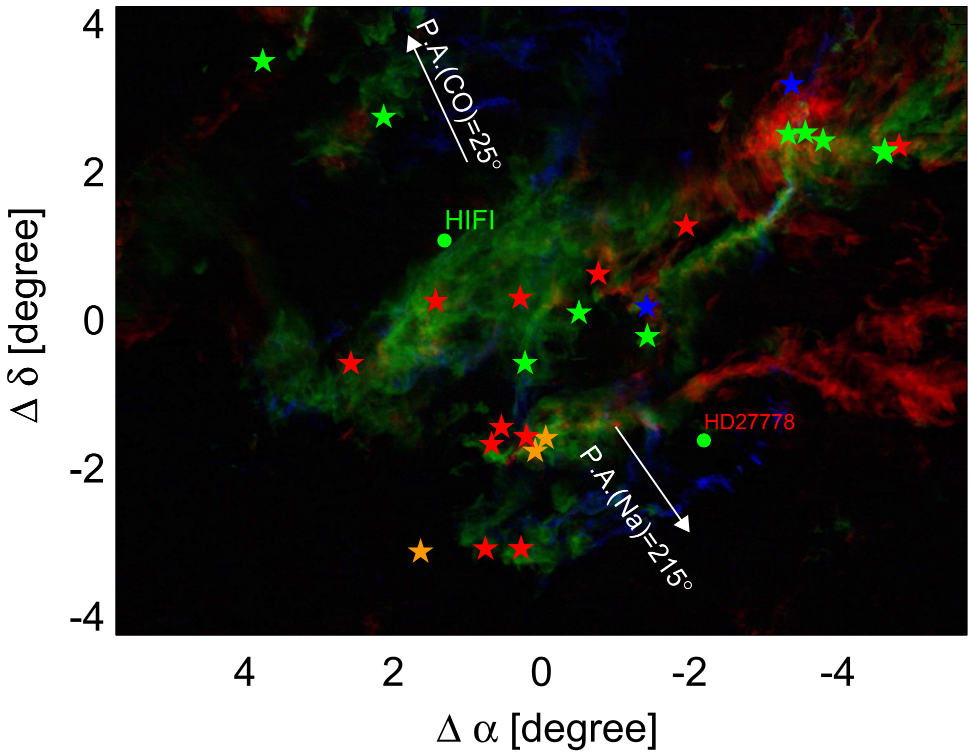

Figure 13. Color-coded image of the ^{13}CO integrated intensity in three LSR velocity intervals: 3–5 km s^{-1} is coded blue, 5–7 km s^{-1} green, and 7–9 km s^{-1} red; see also Goldsmith et al. (2008). Our TTSs are shown with stars, the color-coding representing their Na I RV also in LSR. We included one additional velocity bin (9–11 km s^{-1} LSR, orange) to cover the larger velocity range seen in the Na I and K I absorption lines. White arrows show the position angles of ^{13}CO and the Na I rotation axis; velocity gradients are perpendicular to each axis. Note that the ^{13}CO and the Na I axes are almost antiparallel. The magnetic field direction is at a P.A. of 25° (205°), very similar to the rotation axis of the molecular gas and the Na I gas.

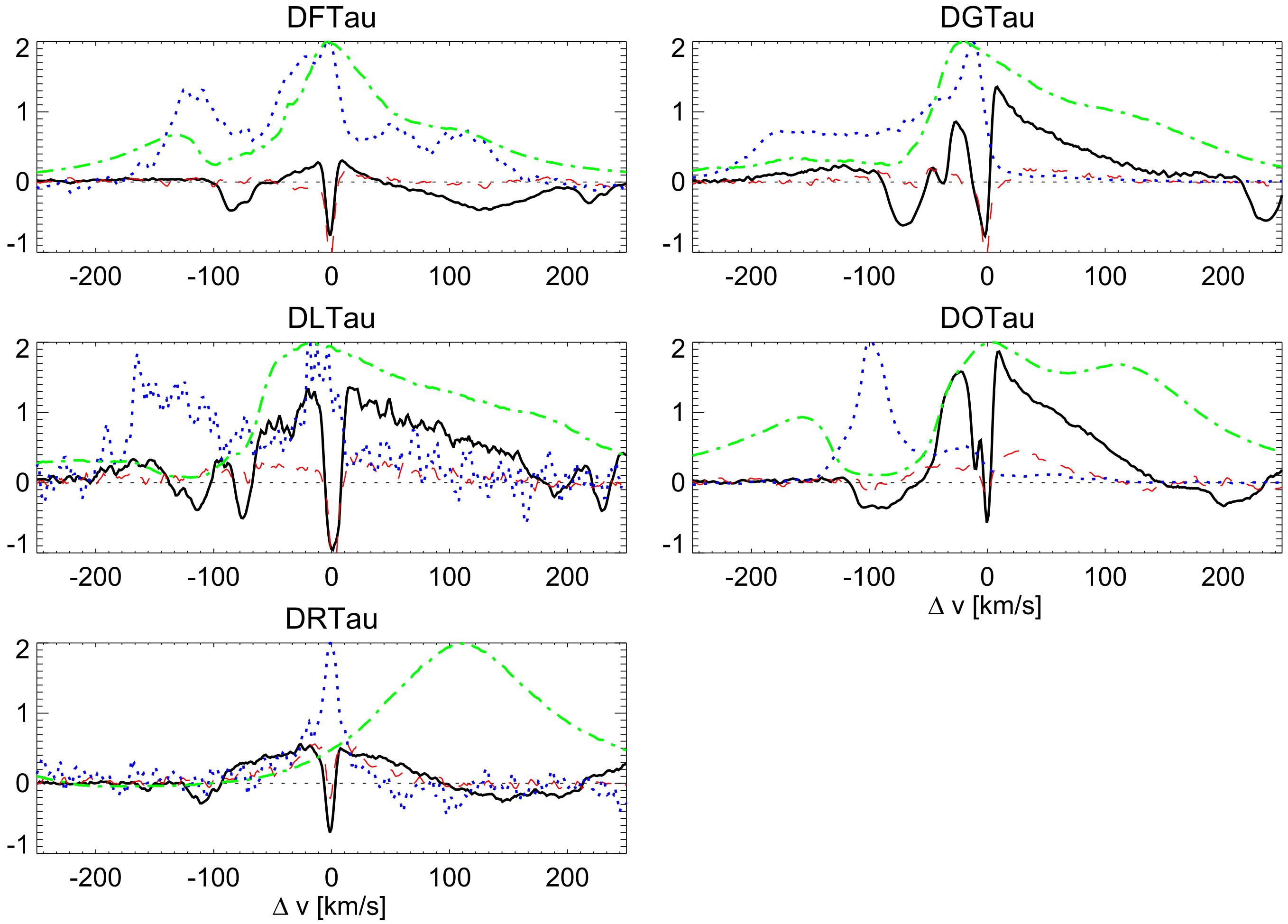

Figure 14. Sources with broad Na I absorptions. A black solid line shows the residual Na I λ5890, profile while a red dashed line shows the K I λ7699 line. Normalized residual profiles for the Hα (green dot-dashed line) and the [O I] λ6300 (blue dotted line) lines are also superimposed. The velocity scale is larger than in previous figures to show both the broad blue- and redshifted absorptions. All velocities are in the stellocentric reference frame.

the direction of HD 27778, and find a distribution peaking at ~0.7 km s^{-1}. Assuming an isotropic turbulence of ~0.5 km s^{-1}, which seems to be common to many lines of sight, implies an atomic gas temperature of ~100 K. Gas as cold as CO (~15 K) would result in b-values much smaller than typically observed. These results suggest that the gas associated with the alkali metals is much warmer than the molecular gas. In models of photodissociation regions, temperatures of several hundred kelvin also trace the transition zone where ionized carbon is converted into atomic carbon. This zone is well outside the cold and FUV-shielded core where most of the hydrogen is in H$_2$ and most of the carbon in CO (e.g., Roellig et al. 2007). Recently, *Herschel*/HIFI observations demonstrated that a significant fraction, between 20% and 75%, of the ISM gas that is undetected in H I and CO is bright in the [C II] FIR line at 158 μm (Langer et al. 2014). Orr et al. (2014) compared [C I], [C II], and CO emission lines toward a linear edge region in the Taurus molecular cloud. While the strength of the [C I] lines is well correlated with that of CO lines (and its ^{13}CO isotoplogue), the [C II] lines are only detected (at a low S/N) in two locations outside of the region where most of the molecular emission occurs (see their Figure 1). A comparison of [C II] peak centroids and Na I and K I absorption toward the same line of sight would be very valuable to test if these transitions probe similar or larger regions.

To summarize, the available data suggest that the Na I and K I absorption lines trace the warm (~100 K) atomic envelope of the cold molecular CO gas in Taurus. Its extent may be comparable to that of the H I 21 cm and/or the [C II] FIR emission. The finding that the rotation axes of the atomic and molecular gas are not aligned is not unique to the Taurus region. Imara & Blitz (2011) compared the velocity gradient P. A. of the molecular (CO) and atomic (H I 21 cm emission) gas of five giant molecular clouds in the Milky Way. Except for Orion A, they find that the positional angles of the molecular and atomic morphological axes are widely separated, by as much as 130° in the case of the Rosetta molecular cloud, and there is no correlation between the atomic and molecular gas rotation axes. Their results demonstrate that giant molecular clouds do not simply inherit their present velocity field from the atomic gas from which they formed and suggest that a disordered or turbulent component may play an important role in setting the rotation axes. Our analysis of Taurus extends this finding to a smaller molecular cloud and shows that Na I and K I resonance absorption lines can also be used to trace the structure of the atomic gas associated with molecular clouds.

5. CONCLUSIONS AND PERSPECTIVES

Narrow Na I absorption resonance lines have long been known to be common in the optical spectra of TTSs. However, their origin remained elusive. Here we have presented a detailed analysis of the Na I and K I resonance lines toward nearly 40 TTSs in Taurus spanning a range of evolutionary stages. Our main findings can be summarized as follows.

1. The peak centroids of the Na I at 5889.95 Å and K I at 7698.96 Å are identical within our velocity uncertainty, and their EWs are positively correlated. This demonstrates that the two transitions trace the same atomic gas.
2. Several of the Na I and K I absorption lines have RVs substantially different from the stellar RV and are detected even toward stars with no circumstellar disks. This demonstrates that Na I and K I do not trace circumstellar disk gas; hence, these features cannot be used to investigate the Na/K ratio in disks, which is relevant for giant exoplanet atmospheres.
3. The Na I and K I RVs have a large spread ($\sim 10\,\mathrm{km\,s^{-1}}$) that cannot be accounted for by gas in the Local Bubble.
4. The distribution of Na I RVs in equatorial coordinates shows a clear gradient, suggesting that the absorption is associated with the Taurus molecular cloud. Assuming that the gradient is due to cloud rotation, the atomic gas rotates along an axis parallel to the magnetic field lines and prograde with respect to differential galactic rotation. This is different from the molecular gas, which is known to have a retrograde motion.
5. The atomic gas traced by Na I and K I absorption lines is more extended and warmer than the molecular gas traced by low-J CO rotational lines.

The almost antiparallel rotation axis between the atomic and molecular gas cannot be explained by simple top-down formation scenarios according to which molecular clouds inherit the velocity field and angular momentum from the rotating galactic disk within which they form. A similar result is found by Imara & Blitz (2011) when analyzing the rotational axes of the atomic and molecular gas from five giant molecular clouds in the Milky Way. In their study, they used the H I 21 cm emission as a tracer of the atomic envelope of molecular clouds. Our results suggest that Na I and K I absorption lines can also be used to trace that atomic gas. A direct comparison of these two different tracers would be extremely valuable. With the *Gaia*-ESO survey acquiring high-resolution UVES spectra of ∼5000 stars in the Milky Way (Smiljanic et al. 2014), Na I and K I absorption lines may be used to trace the kinematic of the atomic gas associated with the molecular gas of several other nearby star-forming regions.

The authors thank D. E. Welty for providing the high-resolution optical spectra toward HD 27778 and J. L. Pineda for sharing the *Herschel* spectra. I.P. would like to thank T. Koskinen and P. Lavvas for stimulating discussions on giant exoplanet atmospheres and L. Hartmann and T. Megeath for helpful discussions on star formation processes. This work was partially supported by an NSF Astronomy & Astrophysics Research Grant (ID: 1312962).

Facility: Keck.

APPENDIX
BROAD Na I AND K I ABSORPTION FEATURES

The five objects with broad Na I absorptions are among the highest accretors in our sample ($\dot{M} \geqslant 10^{-8}\,M_\odot\,\mathrm{yr}^{-1}$; e.g., Gullbring et al. 1998 Hartmann et al. 1998; White & Ghez 2001). As shown in Figure 14, broad absorptions are both on the blue and on the red side of the Na emission. A red absorption at several hundred kilometers per second is a signature of mass infall (e.g., Edwards et al. 1994). Conversely, the broad absorptions located between −150 and $-50\,\mathrm{km\,s^{-1}}$ are most likely associated with material ejected from the star. Blueshifted absorptions are also present in the K I profiles of DG Tau and DO Tau, but they are much weaker than those in the Na I line. The inference of mass ejection is confirmed by the velocity coincidence of these absorption features with absorptions in the Hα line and emission in the [O I] λ6300 line, a known tracer of jets/outflows (e.g., HEG95). We note that in the case of DR Tau the absorption in the Hα line is very shallow and difficult to see with the scaling used in Figure 14, while the [O I] jet emission is more pronounced in the older and lower-resolution spectra by HEG95 (their Figure 5). A notable difference between the blue absorption in the Na I and Hα lines is that the latter are broader, suggesting that Na traces only specific regions along the jet. In addition, the fact that these velocities are smaller than the peak velocities of the forbidden oxygen emission lines indicates that Hα and Na I absorptions mostly trace ambient material shocked to lower speeds.

REFERENCES

Alcalá, J. M., Natta, A., Manara, C. F., et al. 2014, A&A, 561A, 2
Alexander, R., Pascucci, I., Andrews, S., Armitage, P., & Cieza, L. 2014, Protostars and Planets VI, ed. H. Beuther et al. (Tucson, AZ: Univ. Arizona Press), 475
Appenzeller, I., Bertout, C., & Stahl, O. 2005, A&A, 434, 1005
Ballesteros-Paredes, J., Hartmann, L., & Vazquez-Semadeni, E. 1999, ApJ, 527, 285
Barlow, M. J. 1978, MNRAS, 183, 417
Blitz, L. 1993, Protostars and Planets III, 125
Calvet, N., D'Alessio, P., Hartmann, L., et al. 2002, ApJ, 568, 1008
Cieza, L. A., Olofsson, J., Harvey, P. M., et al. 2013, ApJ, 762, 100
Cohen, M., & Kuhi, L. V. 1979, ApJS, 41, 743
Dame, T. M., Hartmann, D., & Thaddeus, P. 2001, ApJ, 547, 792
Duchene, G., Ghez, A. M., McCabe, C., & Weinberger, A. J. 2003, ApJ, 592, 288
Dupree, A. K., Brickhouse, N. S., Cranmer, S. R., et al. 2012, ApJ, 750, 73
Edwards, S., Hartigan, P., Ghandour, L., & Andrulis, C. 1994, AJ, 108, 1056
Edwards, S., Kwan, J., Fischer, W., et al. 2013, ApJ, 778, 148
Espaillat, C., Muzerolle, J., Najita, J., et al. 2014, Protostars and Planets VI, ed. H. Beuther et al. (Tucson: Univ. Arizona Press), 497
Esplin, T. L., Luhman, K. L., & Mamajek, E. E. 2014, ApJ, 784, 126
Farhang, A., Khosroshahi, H. G., Javadi, A., & van Loon, J. Th. 2015, ApJS, 216, 33
Furlan, E., Forrest, W. J., Sargent, B. A., et al. 2009a, ApJ, 706, 1194
Furlan, E., Hartmann, L., Calvet, N., et al. 2006, ApJS, 165, 568
Furlan, E., Luhman, K. L., Espaillat, C., et al. 2011, ApJS, 195, 3
Furlan, E., Watson, D. M., McClure, M. K., et al. 2009b, ApJ, 703, 1964
Ghez, A. M., Neugebauer, G., & Matthews, K. 1993, AJ, 106, 2005
Goldsmith, P. F., Heyer, M., Narayanan, G., et al. 2008, ApJ, 680, 428
Goodman, A. A., Benson, P. J., Fuller, G. A., & Myers, P. C. 1993, ApJ, 406, 528
Gullbring, E., Hartmann, L., Briceno, C., & Calvet, N. 1998, ApJ, 492, 323
Hartigan, P., Hartmann, L., Kenyon, S., Hewett, R., & Stauffer, J. 1989, ApJS, 70, 899
Hartmann, L., Calvet, N., Gullbring, E., & D'Alessio, P. 1998, ApJ, 495, 385

Hartmann, L., Hewett, R., Stahler, S., & Mathieu, R. D. 1986, ApJ, 309, 275
Herczeg, G. J., & Hillenbrand, L. A. 2014, ApJ, 786, 97
Imara, N., & Blitz, L. 2011, ApJ, 732, 78
Ireland, M. J., & Kraus, A. L. 2008, ApJL, 678, L59
Joy, A. H. 1942, PASP, 54, 15
Kenyon, S. J., Brown, D. I., Tout, C. A., & Berlind, P. 1998, AJ, 115, 2491
Kenyon, S. J., Gómez, M., & Whitney, B. A. 2008, in Handbook of Star Forming Regions, Volume I: The Northern Sky, Vol. 4, ed. B. Reipurth (ASP Monograph Publications San Francisco, CA: ASP), 405
Kenyon, S. J., & Hartmann, L. 1995, ApJS, 101, 117
Kleiner, S. C., & Dickman, R. L. 1985, ApJ, 295, 466
Kraus, A. L., Ireland, M. J., Hillenbrand, L. A., & Martinache, F. 2012, ApJ, 745, 19
Langer, W. D., Velusamy, T., Pineda, J. L., Willacy, K., & Goldsmith, P. F. 2014, A&A, 561A, 122
Lavvas, P., Koskinen, T., & Yelle, R. V. 2014, ApJ, 796, 15
Mamajek, E. E. 2005, ApJ, 634, 1385
Martin, E. L., & Magazzu, A. 1999, A&A, 342, 173
McJunkin, M., France, K., Schneider, P. C., et al. 2014, ApJ, 780, 150
Mooley, K., Hillenbrand, L., Rebull, L., Padgett, D., & Knapp, G. 2013, ApJ, 771, 110
Mundt, R. 1984, ApJ, 280, 749
Muzerolle, J., Hartmann, L., & Calvet, N. 1998, AJ, 116, 455
Narayanan, G., Heyer, M. H., Brunt, C., et al. 2008, ApJS, 177, 341
Natta, A., & Giovanardi, C. 1990, ApJ, 356, 646
Natta, A., Testi, L., Alcala, J. M., et al. 2014, A&A, 569A, 5
Nguyen, D. C., Brandeker, A., van Kerkwijk, M. H., & Jayawardhana, R. 2012, ApJ, 745, 119
Nguyen, D. C., Jayawardhana, R., van Kerkwijk, M. H., et al. 2009, ApJ, 695, 1648
Orr, M. E., Pineda, J. L., & Goldsmith, P. F. 2014, ApJ, 795, 26
Press, W. H., Flannery, B. P., Teukolsky, S. A., & Vetterling, W. T. 1993, Numerical Recipes in FORTRAN (Cambridge: Cambridge Univ. Press)
Ray, T., Dougados, C., Bacciotti, F., Eisloffel, J., & Chrysostomou, A. 2007, in Protostars and Planets V, ed. B. Reipurth, D. Jewitt & K. Keil (Tucson: Univ. Arizona Press), 231
Redfield, S., & Linsky, J. L. 2008, ApJ, 673, 283
Rivera, J. L., Loinard, L., Dzib, S. A., et al. 2015, ApJ, 807, 119
Roellig, M., Abel, N. P., Bell, T., et al. 2007, A&A, 467, 187
Rucinski, S. M., Matthews, J. M., Kuschnig, R., et al. 2008, MNRAS, 391, 1913
Shu, F. H., Adams, F. C., & Lizano, S. 1987, ARA&A, 25, 23
Shuter, W. L. H., Dickman, R. L., & Klatt, C. 1987, ApJ, 322L, 103
Sing, D. K., Wakeford, H. R., Showman, A. P., et al. 2015, MNRAS, 446, 2428
Smiljanic, R., Korn, A. J., Bergemann, M., et al. 2014, A&A, 570A, 122
Steffen, A. T., Mathieu, R. D., Lattanzi, M. G., et al. 2001, AJ, 122, 997
Torres, C. A. O., Quast, G. R., Melo, C. H. F., & Sterzik, M. F. 2008, in Handbook of Star Forming Regions, Volume II: The Southern Sky, Vol. 5, ed. B. Reipurth (ASP Monograph Publications San Francisco, CA: ASP), 757
Vogt, S. S., Allen, S. L., Bigelow, B. C., et al. 1994, Proc. SPIE, 2198, 362
Welty, A. D. 1995, AJ, 110, 776
Welty, D. E., & Hobbs, L. M. 2001, ApJS, 133, 345
White, R. J., & Ghez, A. M. 2001, ApJ, 556, 265
Wichmann, R., Krautter, J., Schmitt, J. H. M. M., et al. 1996, A&A, 312, 439
Woitas, J. 2003, A&A, 406, 685